Electronic Supplementary Information

Activation of cGAS-STING pathway by a mitochondrial DNA-targeted emissive rhodium(III) metallointercalator

Yue Zheng,‡[a] Xiao-Xiao Chen,‡[a] Dong-Yang Zhang,[a] Wen-Jin Wang,[a] Kun Peng,[a] Zhi-Yuan Li,[a] Zong-Wan Mao*[a] and Cai-Ping Tan*[a]

[a] MOE Key Laboratory of Bioinorganic and Synthetic Chemistry, School of Chemistry, State Key Laboratory of Oncology in South China, Sun Yat-Sen University, Guangzhou 510006, P. R. China.

‡: These authors contributed equally to this work.

Email: cesmzw@mail.sysu.edu.cn; tancaip@mail.sysu.edu.cn

Content

Supporting Experimental Methods

Materials and Measurements

Materials: All starting materials were used as received from commercial sources unless otherwise stated. Rhodium chloride hydrate, 2-phenylpyridine (ppy), CDDP, CT-DNA, H_2DCFDA, ethidium bromide (EB), (3-(4,5)-dimethylthiahiazo(-z-y1)-3,5-di-phenytetrazoliumromide, dimethyl sulfoxide (DMSO), Tween80, chloroquine, carbonyl cyanide 3-chlorophenylhydrazone (CCCP), MitoTracker Deep Red (MTDR), Lyso-tracker deep red (LTDR), rhodamine 123 (Rh123), 4',6-diamidino-2-phenylindole dihydrochloride (DAPI), MB and DNase I were purchased from Sigma Aldrich (USA). PicoGreen, Coomassie Brilliant Blue G-250 Dye (CBB), Trizol, SequalPrep™ Long PCR Kit, Mitochondria isolation kit and Halt Phosphatase Inhibitor Single-Use Cocktail were purchased from Thermo Scientific (USA). z-VAD-fmk, Necrostatin-1, Cycloheximide and 3-Methyladenine (3-MA) were purchased from Selleck (USA). Nucleoprotein extraction kit, radio immunoprecipitation assay (RIPA), Trypan blue, bicinchoninic acid (BCA) protein quantification kit and Hematoxylin-Eosin (H&E) staining kit were purchased from Beyotime (China). Granulocyte-macrophage colony-stimulating factor (GM-CSF, R&D, USA), IL-4 (Pepreotech, USA), Collagenase IV (Worthington, USA), Amersham ECL Prime Western Blotting Detection Reagent (GE Healthcare, USA) were purchased from commercial sources. Quick-gDNA MiniPrep kit was purchased from ZYMO Research (D3025, USA). AxyPrep Blood gDNA MiniPrep kit was purchased from Corning (USA). SYBR Green I Master kit and RT-PCR and Transcriptor First Strand cDNA Synthesis Kit were purchased from Roche (USA). Cellular ATP quantification assay kit was purchased from Promega (USA). Annexin V apoptosis detection kit was purchased from Biolegend (USA). Fixable viability stain 450 (FVS450-BV421) was purchased from BD Pharmingen (USA). Seahorse XF Cell Mito Stress Test Kit and Glycolysis Stress Test Kit were purchased from Agilent Technologies (USA). SAM and SAH ELISA Combo Kit was purchased from Cell Biolabs (USA). 2'3'-cGAMP ELISA kit was purchased from Cayman (USA). IFN-α and IFN-β ELISA kits were purchased from

ELK Biotechnology (China). IFN-γ, Perforin 1, Granzyme B, TNF-α, IL-1β and IL6 ELISA kits were purchased from Elabscience (China). Red blood cells lysis kit was purchased from Solarbio (China). CD11c MicroBeads UltraPure Kit was purchased from Miltenyi Biotec (Germany). Tissue Protein Extraction Kit was purchased from Bestbio (China). Intracellular Fixation and Permeabilization Kit was purchased from eBioscience (USA). Female BALB/c nude mice were purchased from GemPharmatech CoLtd (China). Complexes were dissolved in DMSO just before the experiments, and the concentration of DMSO in biological experiments was 1% (v/v).

Antibodies including anti-8-OG (Abcam, ab206461), anti-5mC (Abcam, ab214727), anti-5hmC (Abcam, ab214728), horseradish peroxidaseconjugated (HRP)-conjugated anti-mouse/rabbit antibody (Abcam, ab205719/ab6721), DyeLight 488-conjugated anti-mouse antibody (Abcam, ab150113), anti-Bcl-2 (ImmunoWay, YM3041), anti-p53 (ImmunoWay, YTC528), anti-Bax (ImmunoWay, YM3619) , anti-caspase-9 (ImmunoWay, YM3077), anti-cleaved caspase-9 (ImmunoWay, 9505), anti-caspase-3 (ImmunoWay, D3R6Y), anti-STING (Cell Signaling Technology, 13647), anti-phospho-STING (Ser366; rabbit, Cell Signaling Technology, 50907), anti-phospho-STING (Ser365; Cell Signaling Technology, 62912), anti-cGAS (Cell Signaling Technology, 31659), anti-IκB-α (Cell Signaling Technology, 4814S), anti-phospho-IκB-α (Ser32; Cell Signaling Technology, 2859S), anti-IKK-β (Cell Signaling Technology, 2678S), anti-phospho-IKK-α/β (Ser176/180; Cell Signaling Technology, 2697S), anti-vinculin HRP-conjugated antibody (Cell Signaling Technology, 18799). FITC anti-mouse CD11c antibody (N418, Biolegend, 117305), PE anti-mouse CD86 antibody (GL-1, Biolegend, 105007), APC anti-mouse CD80 antibody (16-10A1, Biolegend, 104713), FITC anti-mouse CD3 antibody (17A2, Biolegend, 100203), BV421 anti-mouse CD4 (RM4-4, Biolegend, 116023) and PE anti-mouse Foxp3 antibody (MF-14, Biolegend, 126403) were purchased from commercial resources.

ESI-MS was recorded on a Thermo Finnigan LCQ DECA XP spectrometer (USA). ^{1}H NMR spectra and ^{13}C NMR spectra were recorded on a Bruker AVANCE 400 spectrometer (Germany). Referencing is relative to tetramethylsilane. Elemental analysis was carried out using an Elemental Vario EL CHNS analyzer (Germany).

UV/Vis spectra were recorded on a Varian Cary 300 spectrophotometer (USA). Fluorescent emission spectra were conducted on an FLS 980 steady state spectrometer (UK). Cell imaging experiments were carried out on a Carl Zeiss LSM710 confocal microscope (Germany). Polymerase chain reaction (PCR) was performed using a Roche LightCycler 480 Detection System (Roche, USA). Flow cytometry was conducted on a BD FACS Calibur™ flow cytometer (USA). OCR and ECAR were detected by a Seahorse XFe24 analyzer (USA). The contents of Rhodium in cells were detected by an X Series 2 ICP-MS (USA). Untargeted metabolome profiling was tested by an Agilent 7890 gas chromatograph system coupled with a Pegasus 4D TOF-MS (USA).

Synthesis of Rh1−Rh3 and Rh-Mito: The precursor ($[(ppy)_2Rh(\mu\text{-}Cl)]_2$[1] and N^N ligands (dpq, dppz and dppn)[2] were synthesized according to the literature methods. $[(ppy)_2Rh(\mu\text{-}Cl)]_2$ (0.205 mmol) and N^N ligands (0.420 mmol) were dissolved in CH_3OH/CH_2Cl_2 (1:2, v/v). Then, the mixture was heated to reflux for 6 h under the protection of nitrogen in the dark. 10-folds excess NH_4PF_6 was added and stirred for 1 h. The crude product was obtained by filtration. After purified by column chromatography on silica gel eluted with CH_3OH/CH_2Cl_2/n-hexane. rhodium(III) complexes were obtained as yellow or orange powder.

$[Rh(ppy)_2(phen)]PF_6$ (**Rh1**): Complex **Rh1** was obtained as pale yellow powder. Yield: 96 mg (64%). ^{1}H NMR (400 MHz, DMSO-d_6, ppm) δ = 8.85 (d, J = 8.2 Hz, 2H), 8.33 – 8.24 (m, 4H), 8.00 (dd, J = 18.3, 7.7 Hz, 4H), 7.90 (d, J = 5.3 Hz, 2H), 7.69 (t, J = 6.5 Hz, 2H), 7.58 (d, J = 5.7 Hz, 2H), 7.20 (t, J = 6.6 Hz, 2H), 7.09 (t, J = 7.5 Hz, 2H), 6.98 (t, J = 7.4 Hz, 2H), 6.21 (d, J = 7.6 Hz, 2H). ^{13}C NMR (126 MHz, DMSO-d_6, ppm) δ = 167.57, 167.31, 164.13, 154.09, 149.37, 148.85, 143.70, 140.02, 138.92, 132.11, 130.00, 128.09, 124.90, 124.41, 123.97, 123.25, 120.26. ESI-MS m/z (CH_3OH): calculated for $[M-PF_6]^+$ ($C_{34}H_{24}N_4Rh$) 591.11, found 591.36. Elemental analysis calcd (%) for $C_{34}H_{24}F_6N_4PRh$: C, 55.45; H, 3.28; N, 7.61; found: C, 55.62; H, 3.44; N, 7.80.

[$Rh(ppy)_2(dpq)]PF_6$ (**Rh2**): Complex **Rh2** was obtained as pale yellow powder. Yield: 85 mg (53%). ^{1}H NMR (400 MHz, DMSO-d_6, ppm) δ = 9.70 (d, J = 8.3 Hz, 2H), 9.35 (s, 2H), 8.36 (d, J = 5.0 Hz, 2H), 8.30 (d, J = 8.2 Hz, 2H), 8.19 (dd, J = 8.3, 5.0 Hz, 2H), 8.05 – 7.94 (m, 4H), 7.55 (d, J = 5.7 Hz, 2H), 7.14 (t, J = 7.5 Hz, 2H), 7.04 (q, J = 7.9, 7.3 Hz, 4H), 6.30 (d, J = 7.6 Hz, 2H). ^{13}C NMR (126 MHz, DMSO-d_6, ppm) δ = 167.05, 166.79, 164.10, 151.30, 149.44, 146.67, 143.92, 139.34, 138.88, 135.15, 132.23, 130.05, 129.50, 127.85, 124.93, 123.86, 123.40, 120.18. ESI-MS m/z (CH_3OH): calculated for $[M-PF_6]^+$ ($C_{36}H_{24}N_6Rh$) 643.11, found 643.32. Elemental analysis calcd (%) for $C_{36}H_{24}F_6N_6PRh\cdot H_2O$: C, 53.61; H, 3.25; N, 10.42; found: C, 53.32; H, 3.11; N, 10.61.

[$Rh(ppy)_2(dppz)]PF_6$ (**Rh3**): Complex **Rh3** was obtained as yellow powder. Yield: 98 mg (57%). ^{1}H NMR (400 MHz, DMSO-d_6, ppm) δ = 9.74 (d, J = 8.2 Hz, 2H), 8.47 (dd, J = 7.5, 3.3 Hz, 2H), 8.33 (dd, J = 13.2, 6.6 Hz, 4H), 8.17 (dd, J = 8.5, 5.0 Hz, 4H), 8.06 – 7.95 (m, 4H), 7.63 (d, J = 5.8 Hz, 2H), 7.10 (ddt, J = 28.9, 15.0, 7.5 Hz, 6H), 6.31 (d, J = 7.6 Hz, 2H). ^{13}C NMR (126 MHz, DMSO-d_6, ppm) δ = 167.01, 166.75, 164.12, 151.36, 149.46, 147.99, 143.90, 141.94, 140.08, 138.92, 135.42, 132.48, 132.20, 130.07, 129.41, 128.07, 124.95, 123.86, 123.42, 120.21. ESI-MS m/z (CH_3OH): calculated for $[M-PF_6]^+$ ($C_{40}H_{26}N_6Rh$) 693.13, found 693.47. Elemental analysis calcd (%) for $C_{40}H_{26}F_6N_6PRh$: C, 57.29; H, 3.13, N, 10.02; found: C, 57.41; H, 3.22; N, 9.88.

[$Rh(ppy)_2(dppn)]PF_6$ (**Rh-Mito**): Complex **Rh-Mito** was obtained as orange powder. Yield: 113 mg (62%). ^{1}H NMR (400 MHz, DMSO-d_6, ppm): δ = 9.57–9.52 (m, 2H, $H_l/H_{l'}$), 9.02–8.93 (m, 2H, $H_a/H_{a'}$), 8.37–8.30 (m, 6H, $H_n/H_{n'}/H_d/H_{d'}/H_c/H_{c'}$), 8.11–8.00 (m, 6H, $H_j/H_{j'}/H_s/H_{s'}/H_b/H_{b'}$), 7.71 (m, 2H, $H_m/H_{m'}$), 7.63 (m, 2H, $H_i/H_{i'}$), 7.19–7.15 (m, 4H, $H_u/H_{u'}/H_v/H_{v'}$), 7.08–7.04 (t, 2H, $^3J_{Hh,Hg/Hi;\ Hh',Hg'/Hi'}$ = 8.0 Hz, $H_h/H_{h'}$), 6.34–6.32 (d, 2H, $^3J_{Hg,Hh;\ Hg',Hh'}$ = 8.0 Hz, $H_g/H_{g'}$). ^{13}C NMR (126 MHz, DMSO-d_6, ppm): δ = 167.02 ($C_e/C_{e'}$), 166.76 ($C_q/C_{q'}$), 164.16 ($C_l/C_{l'}$), 151.38 ($C_a/C_{a'}$), 149.55 ($C_r/C_{r'}$), 148.45 ($C_f/C_{f'}$), 143.90 ($C_c/C_{c'}$), 140.75 ($C_k/C_{k'}$), 139.00 ($C_n/C_{n'}$), 137.72 ($C_p/C_{p'}$), 135.27 ($C_t/C_{t'}$), 134.39 ($C_j/C_{j'}$), 132.22 ($C_i/C_{i'}$), 130.33 ($C_o/C_{o'}$), 130.10 ($C_u/C_{u'}$), 128.46 ($C_v/C_{v'}$), 128.17 ($C_h/C_{h'}$), 127.80 ($C_g/C_{g'}$), 125.00 ($C_s/C_{s'}$), 123.93

($C_d/C_{d'}$), 123.45 ($C_m/C_{m'}$), 120.28 ($C_b/C_{b'}$). ESI-MS m/z (CH_3OH): calculated for $[M-PF_6]^+$ ($C_{44}H_{28}N_6Rh$) 743.14, found 743.48. Elemental analysis: calcd (%) for $C_{44}H_{28}F_6N_6PRh \cdot H_2O$: C, 58.29; H, 3.34, N, 9.27; found: C, 58.11; H, 3.39; N, 9.16.

Optical properties: The UV-Vis absorption and emission spectra of rhodium(III) complexes in CH_3CN, CH_2Cl_2 and PBS (10 μM) at 298 K were obtained on a Varian Cary 300 spectrophotometer (USA) and a FLS 980 combined fluorescence lifetime and steady state spectrometer (Japan), respectively.

Stability measurement: Stability studies of the tested rhodium(III) complexes were monitored by UV/Vis spectroscopy. The complexes were firstly dissolved in DMSO and then diluted with culture medium and fetal bovine serum. The absorbance was recorded at time intervals over 0, 12 h, 24 h, 48 h, 72 h at 298 K.

Solubility measurement: Solubility studies of the tested rhodium(III) complexes were monitored by UV/Vis spectroscopy. The complexes were firstly dissolved in DMSO and then diluted with culture medium to 10−100 μM. The absorption spectra were recorded at 298 K and the absorbance of maximum absorptive wavelength at MLCT bands was fitted.

Absorption and fluorescence titration: The experiments were carried out in Tris-HCl buffer (5 mM Tris-HCl, 50 mM NaCl, pH 7.4) at room temperature as previously described.[3] The UV/Vis spectra were recorded on a Varian Cary 300 spectrophotometer (USA). The fluorescence titration was conducted on an FLS 980 steady state spectrometer (UK).

Molecular docking: The docking calculations were performed with AutoDock 4.2 using Lamarckian genetic algorithm method using a double-stranded DNA structure (PDB code: 5IP8). The search space was defined as following: center x = 16.349, center y = 20.209, center z = 14.853; size x = 90, size y = 98, size z = 108; with the spacing

set to 0.375 Å and the exhaustiveness set to 25 iterations. **Rh-Mito** was a mixture of racemic isomers and the structure of **Δ-Rh-Mito** and **Λ-Rh-Mito** was optimized using Gaussian 09 at B3LYP/genecp (SDD basis for rhodium and 6-31G* for other atoms) computation level.

Viscosity measurements: An Ubbelohde viscometer was used to measure the viscosity of CT-DNA (1×10^{-4} M) in the presence of varies concentrations of **Rh-Mito** in a thermostat at 25 °C. The mean values of the relative viscosity of the samples were calculated from three independent measurements according to the formula:

$$\frac{\eta}{\eta_0} = \frac{\rho_0\, t}{\rho_0\, t_0}$$

Cellular protein isolation and electrophoresis: The experiment was carried out as previously described.[4] Briefly, HeLa cells were incubated with **Rh-Mito** (1.0 μM) for different time intervals (2 h, 4 h and 6 h). After the cells were trypsinized and lysed, the concentration of the protein was determined and denatured. The denatured protein was then separated by electrophoresis. The image was taken on a FluorChem M imaging station and analyzed manually with AlphaView software (ProteinSimple, USA).

Cell lines and culture conditions: HeLa, MCF-7, MDA-MB-231, A549, NCI-H1299, HepG2, MCF-10A and HLF cells were obtained from Experimental Animal Center of Sun Yat-Sen University (Guangzhou, China). HeLa-ρ0 cells were kindly provided by Prof. Xingguo Liu at Guangzhou Institutes of Biomedicine and Health, Chinese Academy of Sciences. Cells were routinely maintained in DMEM medium (Dulbecco's modified Eagle's medium, Gibco BRL) and RPMI 1640 (Roswell Park Memorial Institute 1640, Gibco BRL) medium containing 10% FBS (fetal bovine serum, Gibco BRL), 100 μg mL^{-1} streptomycin, and 100 U mL^{-1} penicillin (Gibco BRL). The cells were cultured in a humidified incubator at 37 °C, with an atmosphere of 5% CO_2 and 95% air. HeLa-ρ0 cells were cultured in DMEM with additional uridine and sodium

pyruvate. In each experiment, cells treated with vehicle DMSO (1%, v/v) were used as the reference group.

Cellular uptake and distribution of rhodium(III) complexes by ICP-MS: The intracellular rhodium contents were measured similarly as previously described for iridium quantification using the XSERIES 2 ICP-MS.[4] HeLa, A549, MCF-7, HepG2 and MCF-10A cells were incubated with rhodium(III) complexes (1.0 μM, 1 h) and counted. Mitochondria were isolated using the mitochondria isolation kit (89874, Thermo Scientific). Nuclear and cytosolic fractions were separated using a nucleoprotein extraction kit (C500009, Sangon Biotech, China). RIPA buffer (C500007, Sangon Biotech, China) was used to lyse these fractions.

Cellular uptake mechanism: HeLa cells were incubated at 4 °C and 37 °C for 1 h, or pretreated with 20 μM CCCP or 50 μM Chloroquine for 1 h at 37 °C and then incubated with **Rh-Mito** (1.0 μM) at 37 °C for another 1 h. Cells were washed with PBS and cellular rhodium contents were analyzed by XSERIES 2 ICP-MS.

Colocalization assay: HeLa cells were incubated with **Rh-Mito** (1.0 μM, 1 h) and then stained with MTDR (100 nM) at 37 °C for 15 min. After washed three times with phosphate buffer saline (PBS), the cells were visualized by confocal microscopy immediately. **Rh-Mito**: λ_{ex} = 405 nm; λ_{em} = 620 ± 20 nm. MTDR: λ_{ex} = 633 nm; λ_{em} = 660 ± 20 nm.

Antiproliferation and cytotoxicity assay: The experiment was performed as previously described.[4] Briefly, cells were seeded in 96 well plates and treated with various concentration of **Rh-Mito** or CDDP for 72 h. IC_{50} values and CC_{50} values were calculated using the standard MTT method and Trypan blue method. To investigate the impact of death inhibitors on cell proliferation, HeLa cells were pretreated with the inhibitors (z-VAD-fmk: 50 μM, Necrostain-1: 50 μM, 3-MA: 0.5 mM, Cycloheximide: 1 μM at the indicated concentrations for 1 h).

Colony formation assay: HeLa cells were seeded in 6-well plates and treated with **Rh-Mito** at the indicated concentrations for 7 days. The colonies were washed with PBS, fixed with 4% paraformaldehyde and stained with 0.1% crystal violet. The images were taken on a FluorChem M imaging station.

8-OG immunofluorescence staining: The experiment was performed as previously described.[4] Briefly, HeLa cells were treated with **Rh-Mito** (1.0 μM, 6 h), fixed and incubated with the primary antibody (anti-8-OG) at 4 °C overnight. The cells were then incubated with DyeLight 488-conjugated anti-mouse secondary antibody and stained with DAPI (10 μg mL^{-1}) for 15 min. The cells were observed under a confocal microscopy immediately. 8-OG: λ_{ex} = 488 nm; λ_{em} = 518 ± 20 nm. DAPI: λ_{ex} = 405 nm; λ_{em} = 461 ± 20 nm.

Gel electrophoresis: The experiment was performed as described before [4]. HeLa cells were incubated with **Rh-Mito** at the indicated concentrations for 2 h. MtDNA was extracted and purified by the Quick-gDNA™ MiniPrep kit from isolated mitochondria. Gel electrophoresis of mtDNA was performed on a 1% agarose gel at 100 V for 1 h. After stained with Gel-Red, the image was captured by a FluorChem M imaging station.

Determination of mtDNA copy number and amplification: The experiment was performed as previously described.[4] Briefly, HeLa cells were treated with **Rh-Mito** at the indicated concentrations for 6 h. DNA was extracted and purified by AxyPrep Blood gDNA MiniPrep kit. For mtDNA amplification measurement, DNA was isolated and a SequalPrep™ Long PCR Kit was used to amplify the 8.9 kb segment of mtDNA and the 12.2 kb segment of nucDNA. qPCR was performed using SYBR Green I Master on a Roche LightCycler 480 Detection System. The primer sequences are listed in Table S6.

Transcription of mtDNA-encoded genes: The experiment was performed as previously described.[5] Briefly, HeLa cells were treated with **Rh-Mito** (1.0 μM, 6 h). Total RNA was isolated using the Trizol reagent, First Strand cDNA Synthesis Kit was used to obtain the cDNA template. The following cycling conditions were applied for the RT-qPCR experiment: denature 95 °C for 10 min, followed by 40 cycles of 95 °C for 10 s, 60 °C for 15 s and 72 °C for 20 s. β-actin was used as the housekeeping genes to normalize the data. The primer sequences are listed in Table S6.

Detection of MMP: The experiment was performed as previously described.[4] Briefly, HeLa cells were treated with **Rh-Mito** (1.0 μM) for different time intervals. Then the cells were stained with Rh123 (1 μg mL^{-1}) and analyzed by flow cytometry.

Measurement of intracellular ATP level: The experiment was performed as previously described [4] using the CellTiter-Glo® Luminescent Cell Viability Assay kit. Briefly, HeLa cells were treated with **Rh-Mito** at the indicated concentrations for 6 h. The CellTiter-Glo® reagent was added to each well. The luminescence of each well was measured with a microplate reader (Infinite M200 Pro, Tecan, Switzerland).

Mitochondrial bioenergetics assays: The experiment was performed using the Seahorse XF Cell Mito Stress Test Kit by a Seahorse XFe24 analyzer as previously described.[4] Briefly, HeLa cells were incubated with **Rh-Mito** at the indicated concentrations for 2 h. Then, OCR was measured by the sequential addition of oligomycin (1 μM), trifluoromethoxy carbonylcyanide phenylhydrazone (FCCP, 0.8 μM), a mixture of rotenone (0.5 μM) and antimycin A (0.5 μM). The measurement of ECAR was carried out by the sequential addition of glucose (25 mM), ATP synthase inhibitor oligomycin (1.0 μM) and 2-deoxy-glucose (2-DG, 100 mM).

Annexin V staining: HeLa cells were treated with **Rh-Mito** at the indicated concentrations for 12 h. Cells were washed twice with PBS and stained with antigen presenting cells (APC) Annexin V apoptosis detection kit for 30 min at room

temperature, then stained with Fixable viability stain 450. Cells were analyzed immediately by flow cytometry. At least 10,000 cells were acquired for each sample.

Western blotting: HeLa cells were treated with **Rh-Mito** at the indicated concentrations for 6 h. Cells were harvested and washed with ice-cold PBS twice, then lysed in RIPA buffer supplemented with protease and phosphatase inhibitors. The protein concentration was quantified by BCA protein quantification kit. Equal amounts of cellular total proteins were separated on SDS-PAGE and then transferred onto polyvinylidene difluoride membranes (Roche, USA). Membranes were blocked in 5% BSA and then incubated overnight with primary antibodies at 4 °C. After a subsequent washing step, the membrane was incubated with the appropriate HRP-conjugated secondary antibody. Images were captured using a FluorChem M imaging station and analyzed manually with AlphaView software.

H_2DCFDA/MTDR double staining: HeLa cells were treated with **Rh-Mito** (1.0 μM) for different time intervals (0 h, 0.5 h, 1 h and 2 h), followed by co-incubation with H_2DCFDA (10 μM) and MTDR (100 nM) for 15 min. The cells were observed by confocal microscopy. 2',7'-Dichlorofluorescein (DCF): λ_{ex} = 488 nm, λ_{em} = 520 ± 20 nm. MTDR: λ_{ex} = 633 nm; λ_{em} = 660 ± 20 nm.

PicoGreen/MTDR double staining: HeLa cells were pre-stained with PicoGreen (3 μL mL^{-1}) for 1 h and then stained with MTDR (100 nM) for 15 min. After that, the cells were incubated with **Rh-Mito** (1.0 μM) for different time intervals (0 h, 0.5 h, 1 h and 2 h) and observed by confocal microscopy. PicoGreen: λ_{ex} = 488 nm; λ_{em} = 525 ± 20 nm. MTDR: λ_{ex} = 633 nm; λ_{em} = 660 ± 20 nm.

Co-culture of HeLa cell supernatant and blood-derived DCs: Monocytes were isolated from the peripheral blood of mouse by Ficoll density gradient centrifugation using a literature method.[6] The monocytes were cultured with GM-CSF (50 ng mL^{-1}, R&D, USA) and IL-4 (20 ng mL^{-1}, AF-200-04, Pepreotech, USA) to transform

monocytes into DCs. HeLa cells were treated with **Rh-Mito** at the indicated concentrations for 6 h and the supernatant was separated. The DCs were cultured with the supernatant of HeLa cells for 12 h. The proteins of DCs were extracted for the subsequent assays.

Metabolome profiling: The experiment was carried out as previously described.[7] HeLa cells were treated with **Rh-Mito** (1.0 μM, 6 h). The collected cell pellets were soaked in liquid nitrogen for at least 3 min then stored at −80 °C. The samples were extracted with methanol/chloroform. Using adonitol (0.5 mg mL^{-1}) as the internal standard, the metabolites were analyzed by GC-TOF-MS and peaks were extracted using Chroma TOF 4.3X software and LECO-Fiehn Rtx5 database. Statistical analysis for annotated metabolites was performed using SIMCA-P 14.1. PCA was used to detect trends, and grouping among cases. In OPLS-DA score plots, the variables with variable importance projection (VIP) > 1 were usually regarded as candidate biomarkers for further identification. Metabolism pathways were annotated using KEGG database. Pathway enrichment analysis was conducted with MetaboAnalyst.

Quantitative determination of SAM and SAH by ELISA: HeLa cells were treated with **Rh-Mito** at the indicated concentrations for 6 h. The contents of SAM and SAH were measured by ELISA kits according to the manufacturer's instructions.

Dot blotting assay for 5mC and 5hmC detection: The experiment was done according to the literature method. [8] HeLa or HeLa-ρ0 cells were treated with **Rh-Mito** at the indicated concentrations for 6 h. Total DNA was separated with the DNA extraction Kit. The samples were denatured at 95 °C for 5 min and dotted onto the nylon membrane (RPN119B, GE Healthcare, USA). After UV crosslinking and MB staining, the membrane was washed with PBST, blocked in 5% BSA and incubated with antibodies against antibody (1:1000) or 5hmC antibody (1:1000). After incubated with the HRP-conjugated secondary antibody and developed with the Amersham ECL Prime

Western Blotting Detection Reagent, the membranes were imaged using a FluorChem M imaging station and analyzed manually with AlphaView software.

RRBS and bioinformatics: RRBS was carried out by the literature methods.[9, 10] After HeLa cells were treated with **Rh-Mito** (1.0 μM, 6 h), the isolated genomic DNA was purified by a PureLink genomic DNA kit (Thermo Scientific, USA) and quantified by a Qubit fluorometer (Thermo Scientific, USA) using the dsDNA BR Assay Kit (Thermo Scientific, USA). Then, the MspI-digested genomic DNA was purified and dissolved in EB buffer (10 mM Tris-Cl, pH 8.5). After end repair and "A"-tailing and adapter-ligation, DNA fragments with appropriate size (150−300 bp) was selected by agarose gel electrophoresis, which was treated with bisulfite (EZ DNA Methylation Gold Kit, Zymo Research, USA) to convert the unmethylated cytosine to uracil. RRBS libraries were constructed after PCR. DNA was quantified by a Qubit fluorometer and diluted to 1 ng μL^{-1}. Insert size was assessed using the Agilent Bioanalyzer 2100 system (Agilent Technologies, CA, USA), and qualified insert size was accurate quantified using a StepOnePlus™ Real-Time PCR System. The libraries were sequenced on an Illumina platform and 150 bp paired-end reads were mapped to the reference human genome sequence (NCBI 36.1 [hg19] assembly by TopHat (Version 2.0.6). GO (http://www.geneontology.org/) and KEGG (https://www.kegg.jp/kegg/kegg1.html) of DMRs-anchored promoter region related genes were analyzed (Observed genes > 2, Fold change > 2 and adj $P < 0.05$).

RNA-Seq and bioinformatics: The experiment was carried out as described before by the Biomarker Technologies (China).[3] HeLa cells were treated with **Rh-Mito** (1.0 μM, 6 h), and total RNA was extracted by Trizol reagent and purified using RNeasy mini kit (Qiagen, Germany). The integrity and concentration of RNA was assessed using the RNA Nano 6000 Assay Kit (Agilent Technologies, CA, USA). Sequencing libraries were generated using NEBNext® Ultra™ RNA Library Prep Kit for Illumina® (#E7530L, NEB, USA). RNA concentration of library was measured using Qubit® RNA Assay Kit in Qubit® 3.0 and then diluted to 1 ng μL^{-1}. Insert size was assessed

using the Agilent Bioanalyzer 2100 system (Agilent Technologies, USA), and qualified insert size was accurately quantificatified using the StepOnePlus™ Real-Time PCR System. The libraries were sequenced on an Illumina platform to generate 150 bp paired-end reads, which were mapped to reference human genome sequence hg38 (ftp://ftp.ensembl.org/pub/release-95/fasta/homo_sapiens/dna/) assembled by HISAT (Version 2.0) software. Genes with false discovery rate (FDR) of < 0.05 and > 200 bp were considered as differentially expressed. GSEA was performed following standard procedure (http://www.broadinstitute.org/gsea/doc/GSEAUserGuideFrame.html).

***In vivo* antitumor evaluation:** All animal operations were in accord with the guidelines of Sun Yat-Sen University Animal Care and Use Committee and the approval number is F2022-0300XS. Pathogen-free female BALB/c mice, 4–5 weeks of age, were purchased from GemPharmatech CoLtd, China. The primary tumors were established by subcutaneous injection of U14 cells (1×10^7) into the right axilla. 6 days later, the distant tumors were established by subcutaneous injection of U14 cells (1×10^7) into the left axilla. After 2 days, the mice were randomly divided into four groups (4 mice per group), and **Rh-Mito** (5.0 mg kg^{-1} or 2.0 mg kg^{-1} in solubilizer, DMSO/PEG400/Tween80/saline, 5%, 30%, 5%, 60%, v/v/v/v), CDDP (5.0 mg kg^{-1} in solubilizer) or Control (solubilizer) was intratumorally injected at the sites of the primary tumors. The same treatment was performed every 4 days. The volumes of the both primary and distant tumors were monitored by measuring the perpendicular diameter of the tumors using calipers every two days and calculated according to the formula:

$$\text{Tumor volume (V)} = \frac{(\text{tumor length}) \times (\text{tumor width})^2}{2}$$

For hematoxylin-eosin (H&E) staining, tumor samples and organs were collected and fixed with 4% paraformaldehyde at 4 °C. The samples then were transferred to 10% formalin neutral buffer and embedded in paraffin, stained by H&E and observed under an inverted fluorescence microscope (Zeiss, Germany).

***In vivo* antitumor immunity:** Tumors (n = 3 mice in each group) were made into a single cell suspension using collagenase IV (1 mg mL^{-1}) and DNase I (1 μg mL^{-1}) at 37 °C with agitation in DMEM with 10% FBS. After being filtered through a 70 μm nylon cell strainer, red blood cells were removed by lysis buffer, and DCs were purified by magnetic-activated cell sorting using the CD11c MicroBeads UltraPure Kit according to the manufacturer's instructions. Cells were stained with CD11c-FITC, CD80-APC, CD86-PE, CD8a-APC, CD4-BV421, CD3-FITC or Foxp3-PE and analyzed by flow cytometry.

For intracellular analysis, cells were pretreated with Intracellular Fixation and Permeabilization kit. Protein samples were extracted using the Tissue Protein Extraction Kit. Serums were isolated from mice and stored in liquid nitrogen for analysis. Secretions of IFN-α, IFN-β, IFN-γ, Perforin 1, Granzyme B, TNF-α, IL-1β and IL6 were measured by ELISA kit according to the manufacturer's instructions.

The encapsulation and release of Rh-Mito in recombination human heavy-chain ferritin (HFn) nanocages: The recombinant HFn was produced according to literature methods.[11] Concentration of HFn protein was determined by the BCA assay. The encapsulation of **Rh-Mito** in HFn was performed according to the literature reports.[12] Briefly, HFn solution (1 mg mL^{-1} in 8 M urea solution) was stirred for 30 min at room temperature to ensure complete dissociation. Stock solution of **Rh-Mito** in methanol was added to the reaction mixture to a final concentration of 0.2 mg mL^{-1}. The mixture was transferred to a dialysis bag (Molecular weight cut off: 14 kDa) and dialyzed against gradient concentrations of urea (7, 5, 3, 2, 1 and 0 M, each for 4 h) at 4 °C to obtain the **Rh-Mito@HFn** nanocages. Free **Rh-Mito** were removed by dialyzing the resulting mixture against PBS. The concentration of HFn was determined by the BCA assay. The quantity of the encapsulated **Rh-Mito** was measured by the absorbance at 422 nm. The average diameter of **Rh-Mito@HFn** NPs was measured by dynamic light scattering (DLS, EliteSizer, China) and transmission electron microscope (TEM, JEM-2010HR, Japan)

The time-dependent release of **Rh-Mito** from **Rh-Mito@HFn** NP was determined

by dialyzing the mixture and determining the **Rh-Mito** in the dialysate different pH (6.0 or 7.4) at room temperature.

***In vivo* antitumor properties of Rh-Mito@HFn NPs:** The *in vivo* xenograft model was constructed similarly as described above with modifications. After 4 days of the primary tumor plantation, the mice were randomly divided into four groups (4 mice per group) and intravenously injected with **Rh-Mito@HFn** NPs (5.0 mg kg^{-1} or 2.0 mg kg^{-1} in physiological saline based on the concentrations of **Rh-Mito**), CDDP (5.0 mg kg^{-1} in physiological saline) or Control (physiological saline). After another 4 days, the distant tumors were planted. Tumor volumes and body weights were recorded every 2 days. The contents of immune cells and cytokines were tested as described above.

***In vivo* biological distribution of Rh-Mito@HFn NPs:** U14 tumor-bearing mice were intravenously injected with **Rh-Mito@HFn** NPs (2.0 mg kg^{-1} based on the concentration of **Rh-Mito**) and the tumors were separated after 24 h, 72 h and 14 days treatments. Heart, liver, spleen, lung, kidney and tumor of the mice (n = 3) were minced and dissolved in aqua regia. The concentration of rhodium was measured using the XSERIES 2 ICP-MS.

Statistical analysis: All biological assays were conducted at least thrice with triplicates in each experiment. Statistical analyses were performed with Prism 8.0 (Graph-Pad Software). Statistical significance Figures 2B, C, G, 3C, D, 4F, 5A, 6F, H, K and supplementary Figures S22, S23, S24, S30, S31, S44, S46 was determined using Student's two-tailed *t*-tests (*$p < 0.05$, ** $p < 0.01$, and *** $p < 0.001$).

Supplementary Scheme and Figures

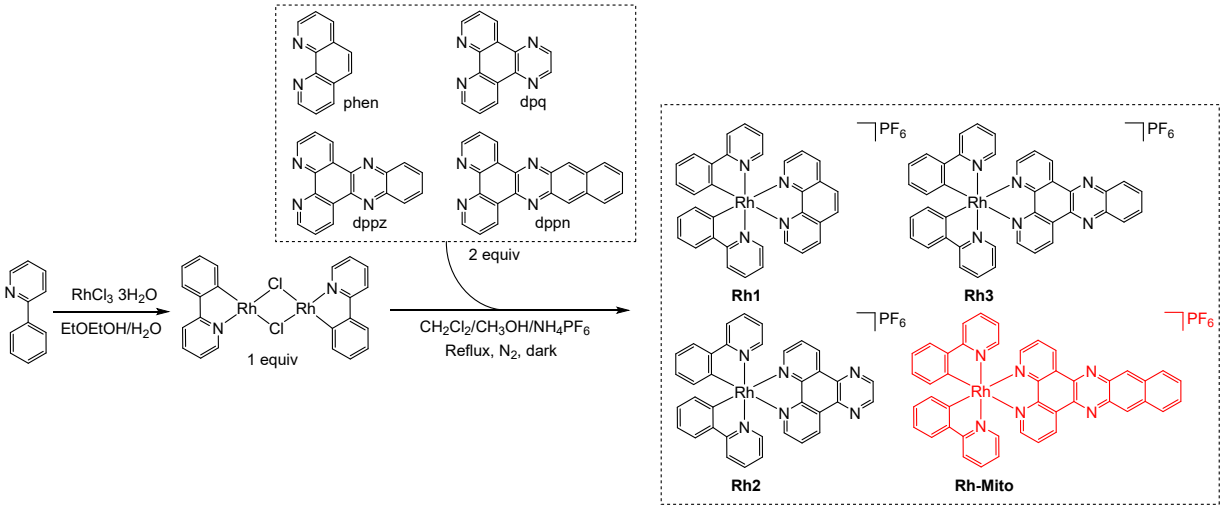

Scheme S1 The synthetic route of rhodium(III) complexes.

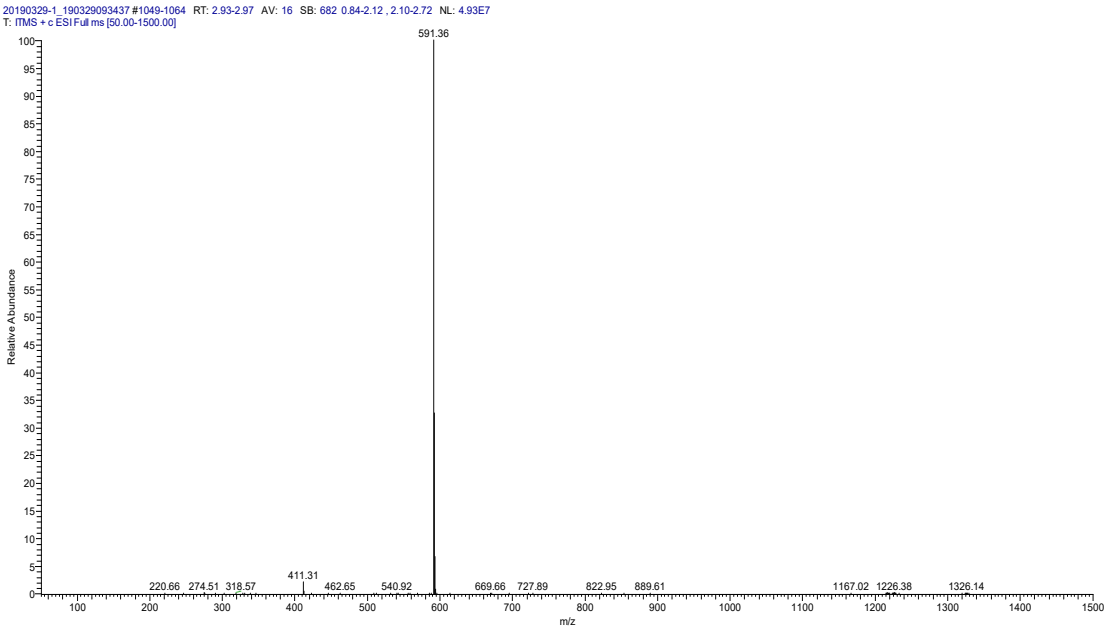

Fig. S1 ESI-MS characterization of **Rh1**.

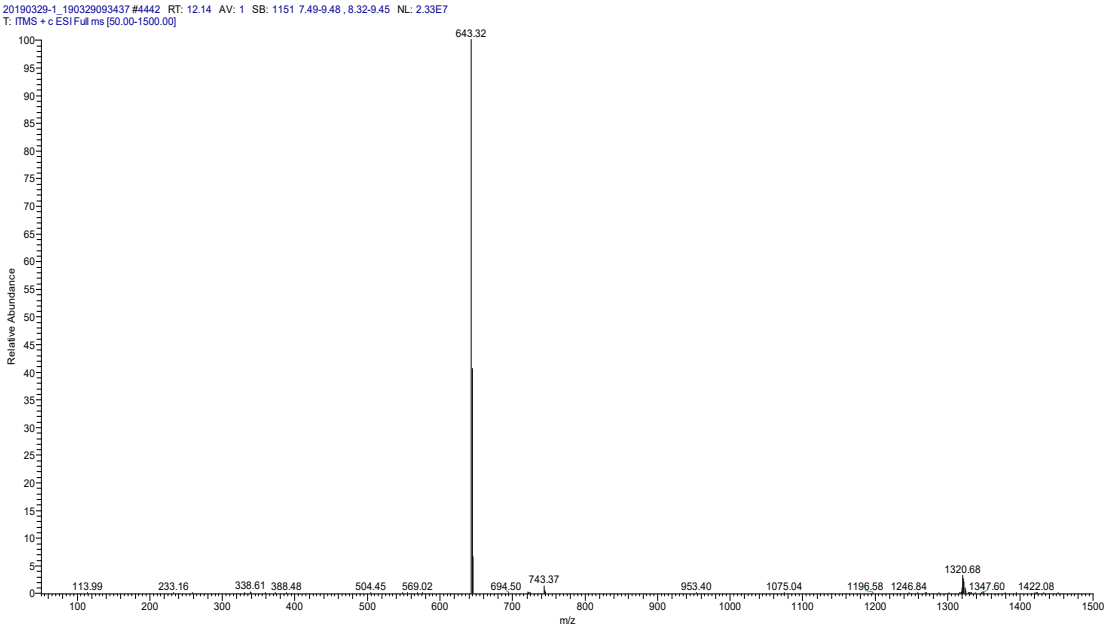

Fig. S2 ESI-MS characterization of **Rh2**.

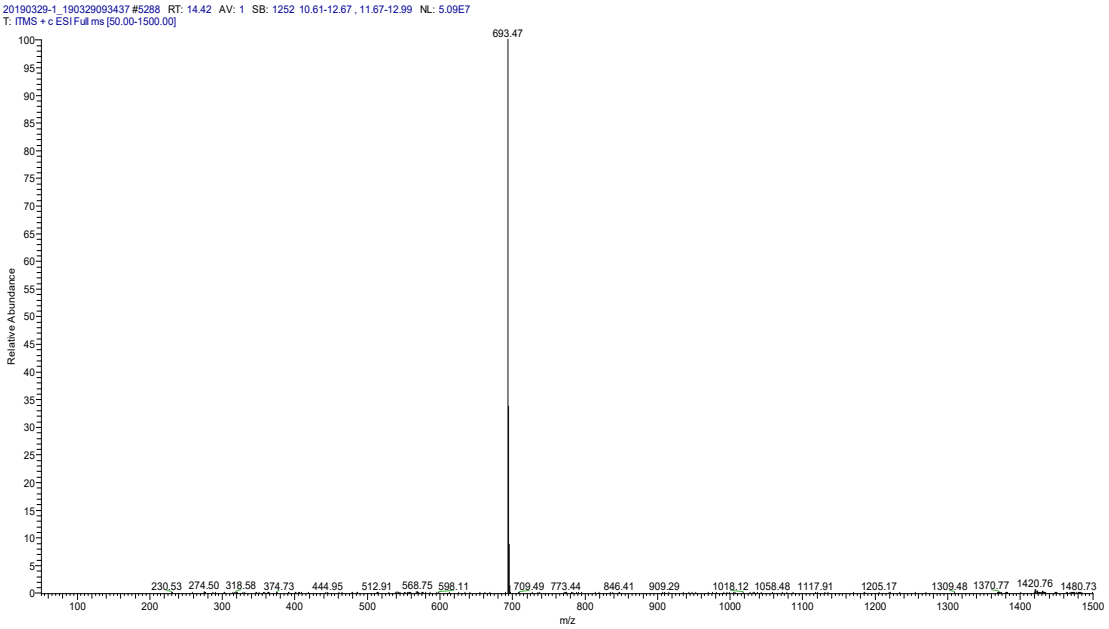

Fig. S3 ESI-MS characterization of **Rh3**.

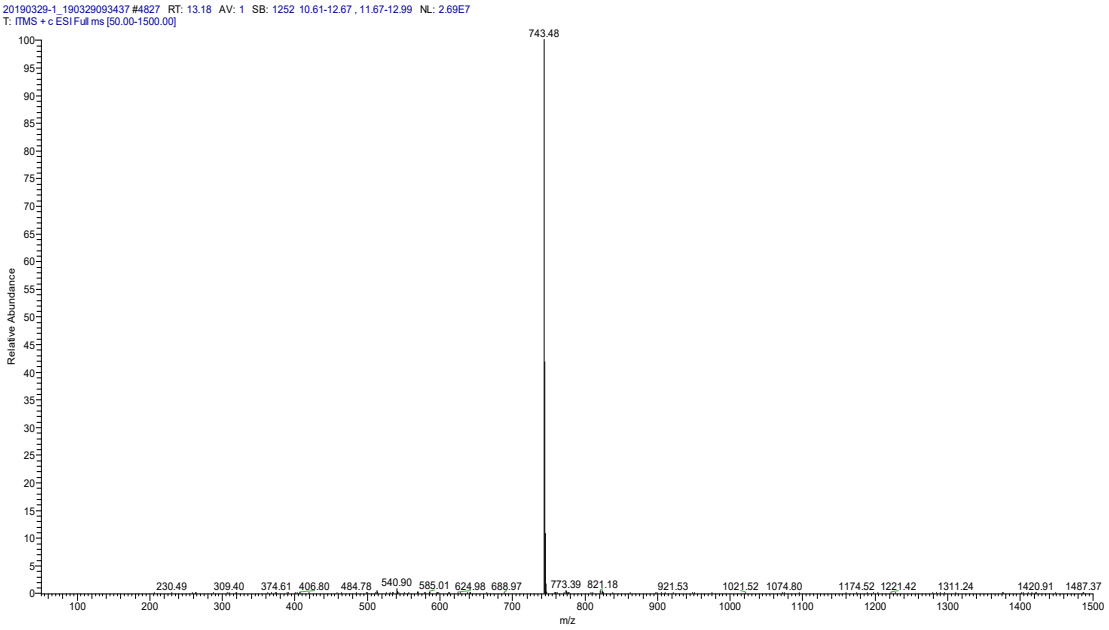

Fig. S4 ESI-MS characterization of **Rh-Mito**.

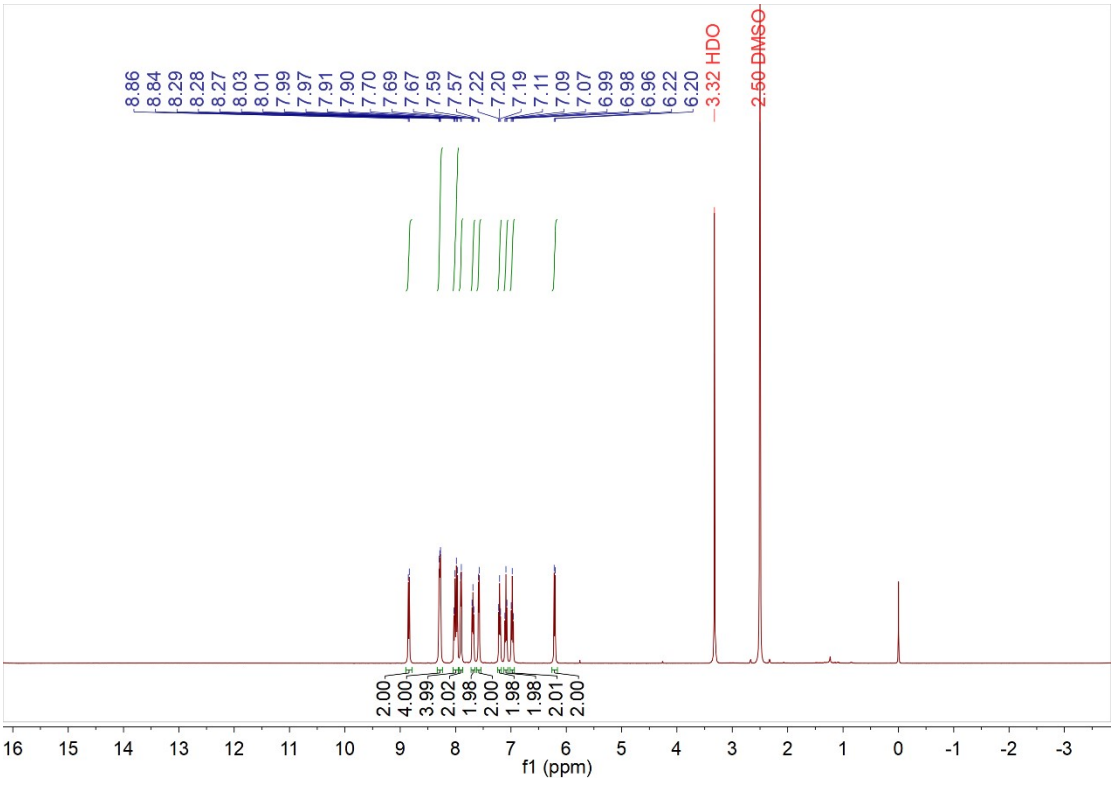

Fig. S5 ^{1}H NMR spectrum of **Rh1**.

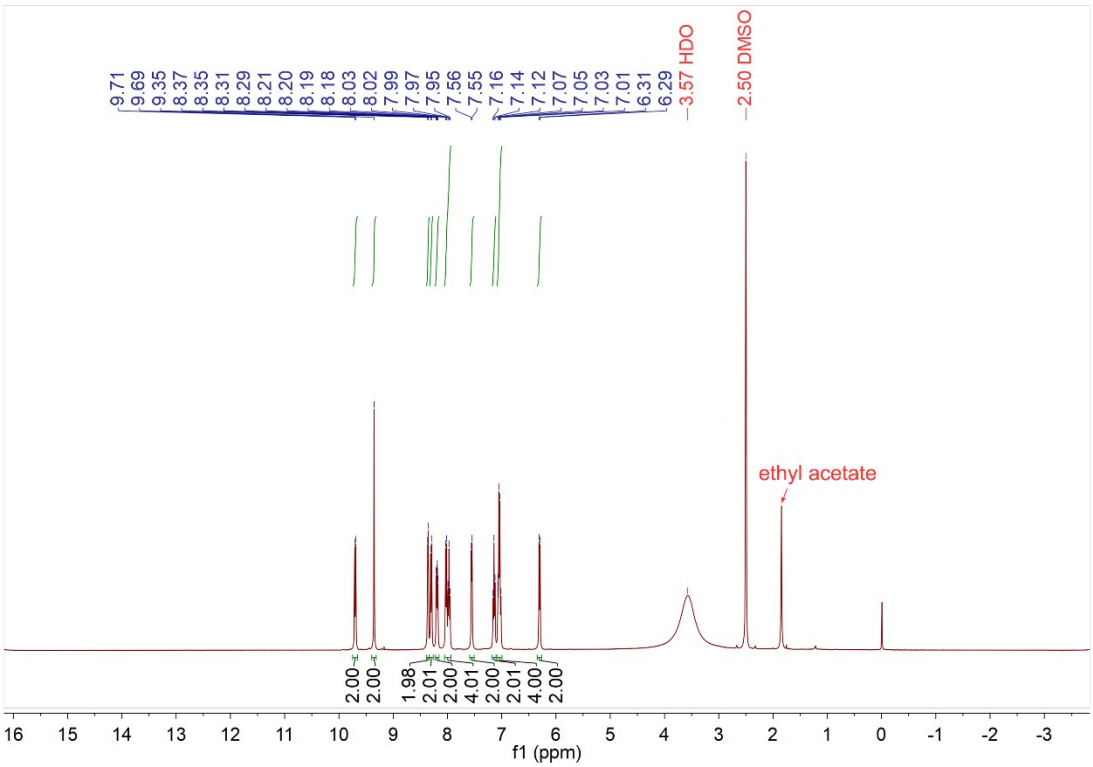

Fig. S6 ^{1}H NMR spectrum of **Rh2**.

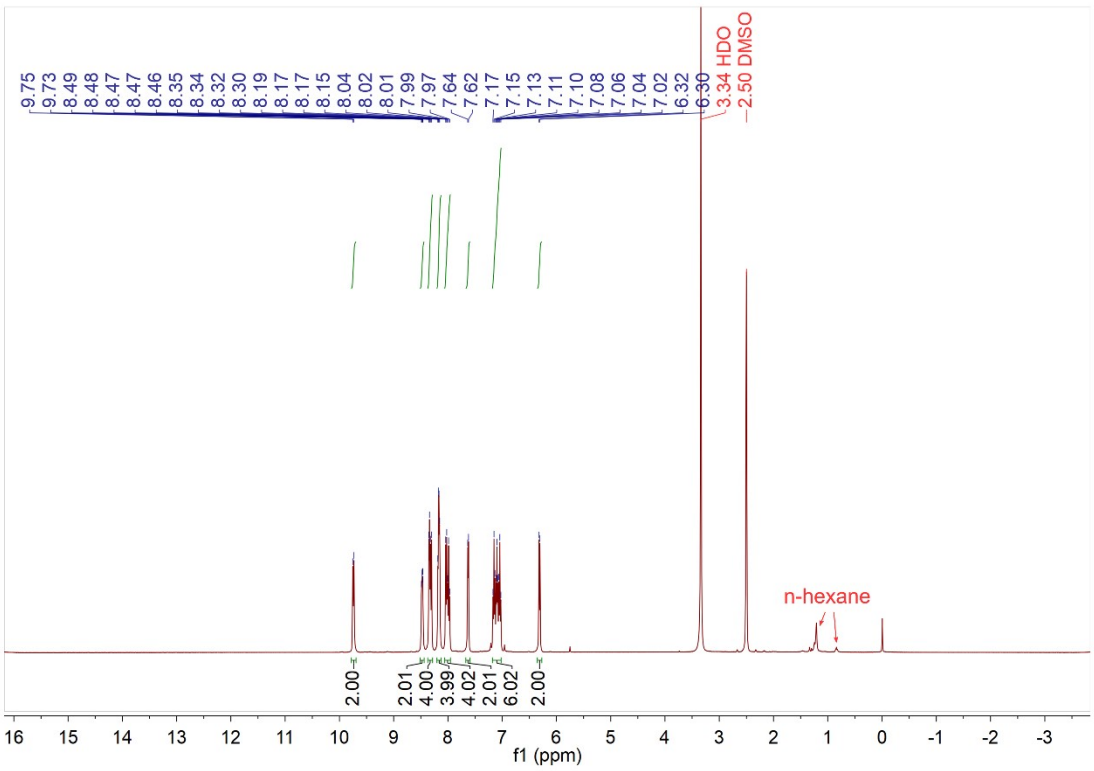

Fig. S7 ^{1}H NMR spectrum of **Rh3**.

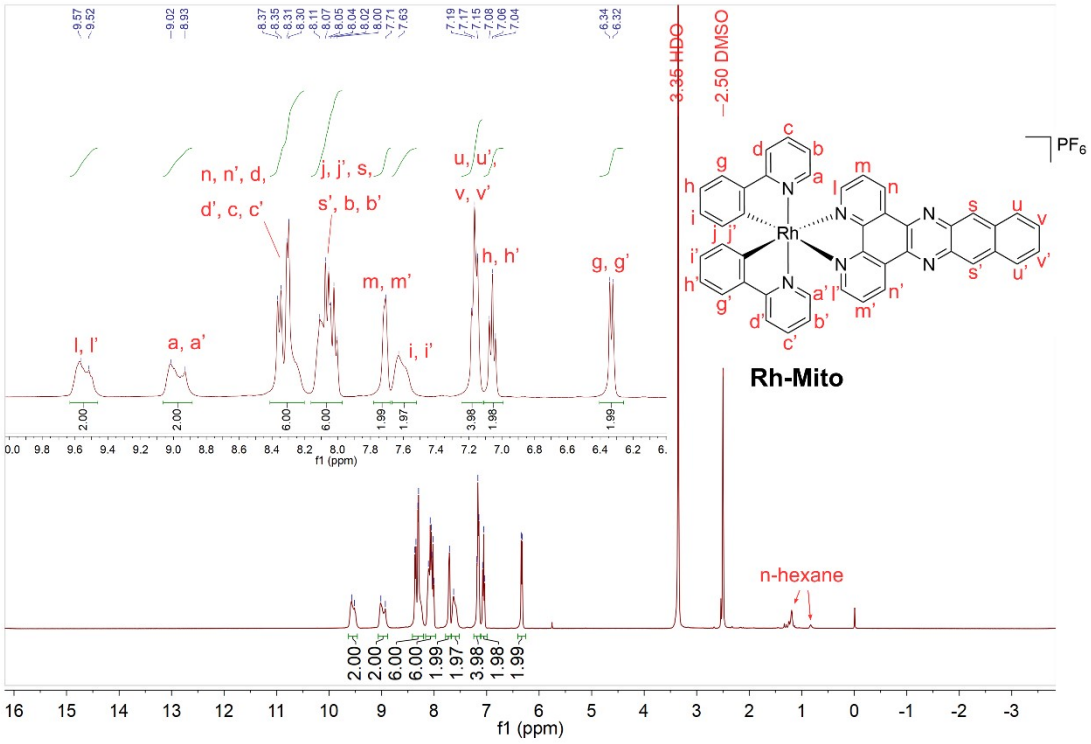

Fig. S8 ^{1}H NMR spectrum of **Rh-Mito**.

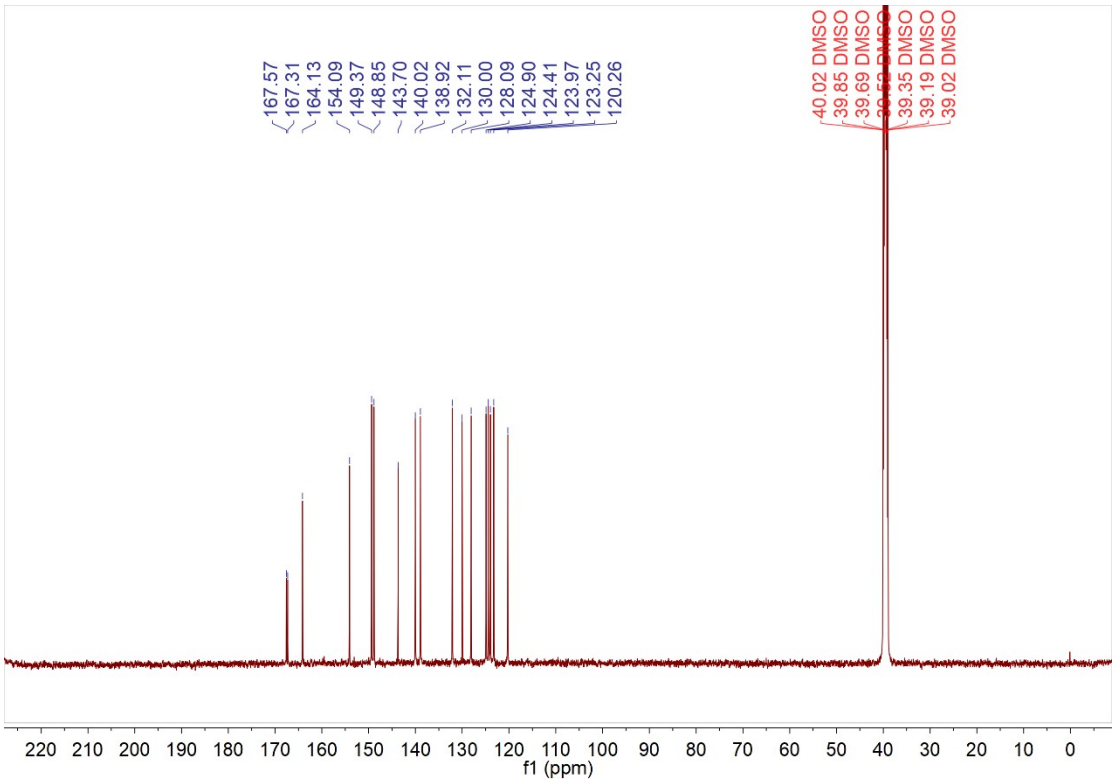

Fig. S9 ^{13}C NMR spectrum of **Rh1**.

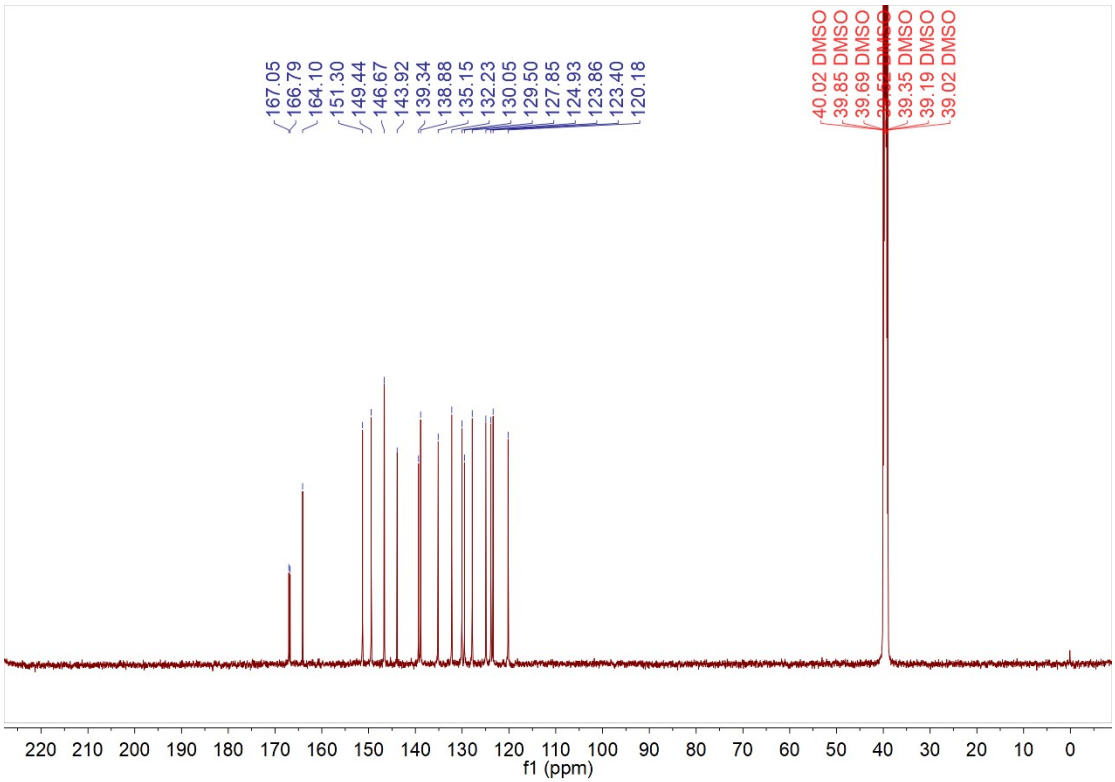

Fig. S10 ^{13}C NMR spectrum of **Rh2**.

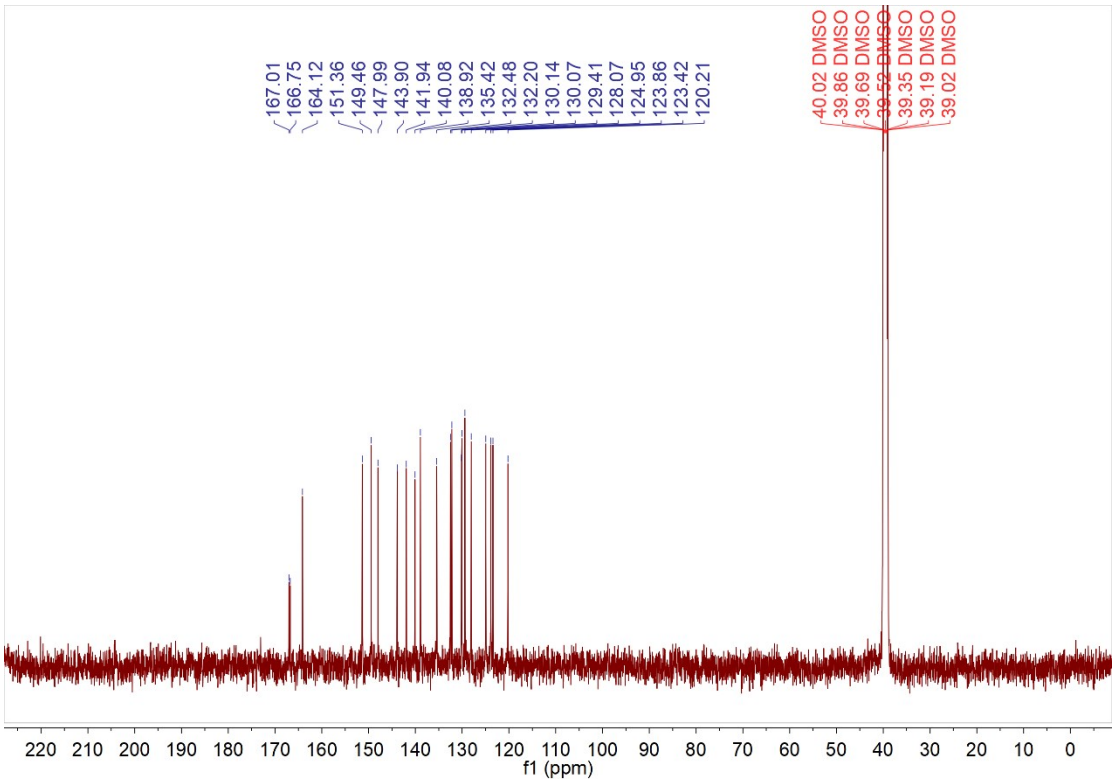

Fig. S11 ^{13}C NMR spectrum of **Rh3**.

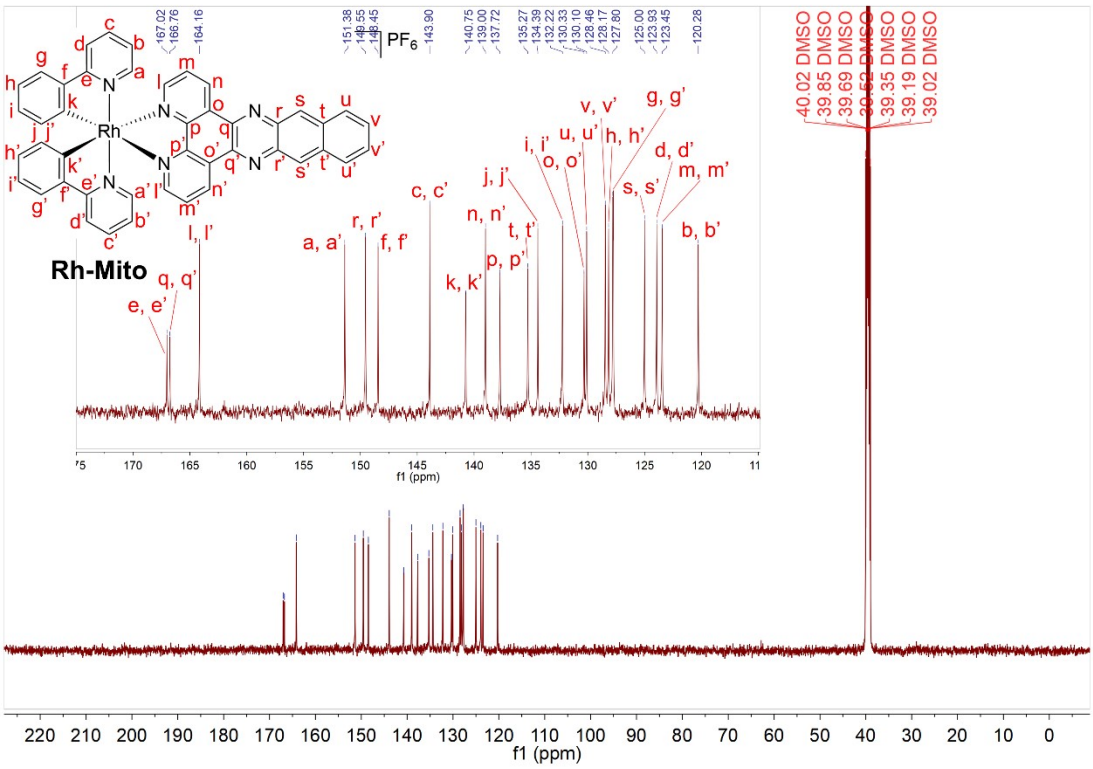

Fig. S12 ^{13}C NMR spectrum of **Rh-Mito**.

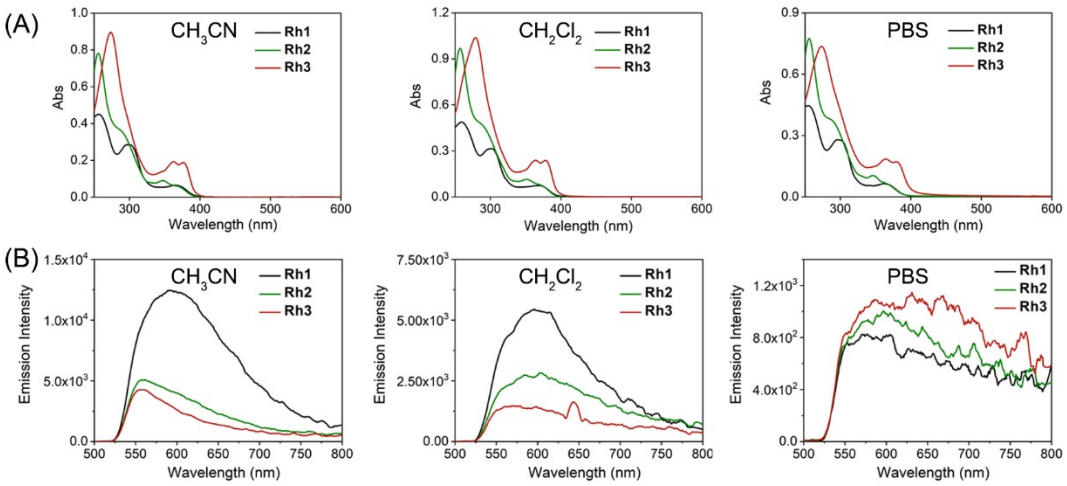

Fig. S13 (A) UV/Vis spectra and (B) emission spectra of **Rh1**–**Rh3** (10 μM) measured in degassed CH_3CN, CH_2Cl_2 and PBS at 298 K.

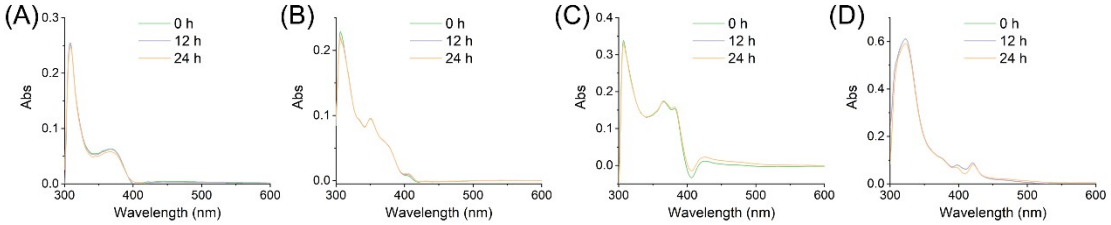

Fig. S14 The stability of rhodium(III) complexes in fetal bovine serum within 24 h measured by UV/Vis spectroscopy.

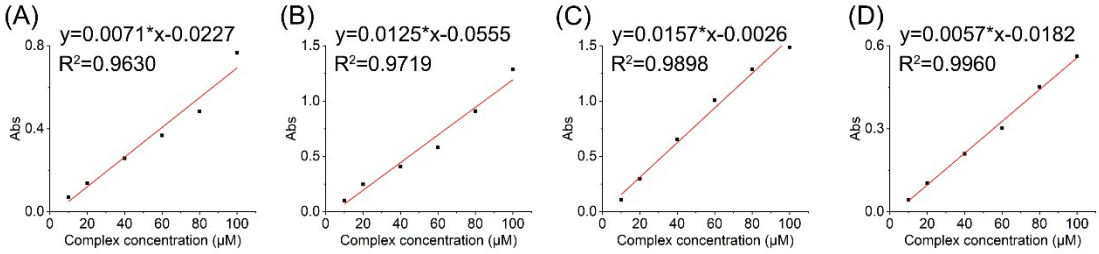

Fig. S15 Fitting curves of the absorbance of (A) **Rh1**, (B) **Rh2**, (C) **Rh3** and (D) **Rh-Mito** at 362 nm, 380 nm, 390 nm and 422 nm *vs* concentration, respectively. Rhodium(III) complexes were dissolved in cell culture medium and 1% DMSO (v/v) was used for solubilization.

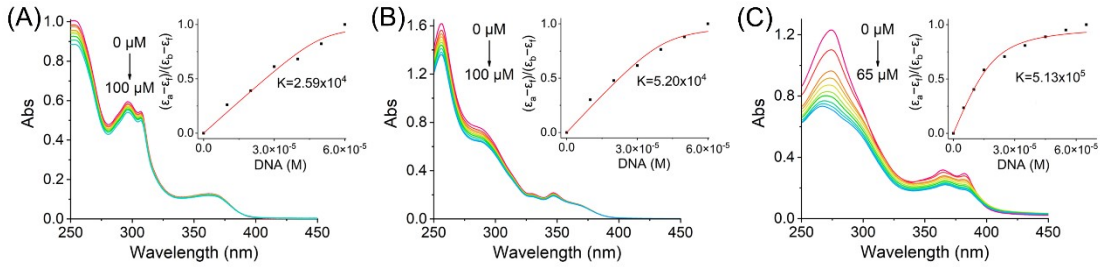

Fig. S16 UV/Vis spectra of (A) **Rh1**, (B) **Rh2** and (C) **Rh3** (10 μM) titrated with CT-DNA (0−100 μM) in Tris-HCl buffer. The arrow shows the alteration in the absorption intensity of **Rh1**−**Rh3** upon the addition of CT-DNA. Insert: Plot of $(\varepsilon_a-\varepsilon_f)/(\varepsilon_b-\varepsilon_f)$ against [DNA] for the binding of **Rh1**−**Rh3** to CT-DNA.

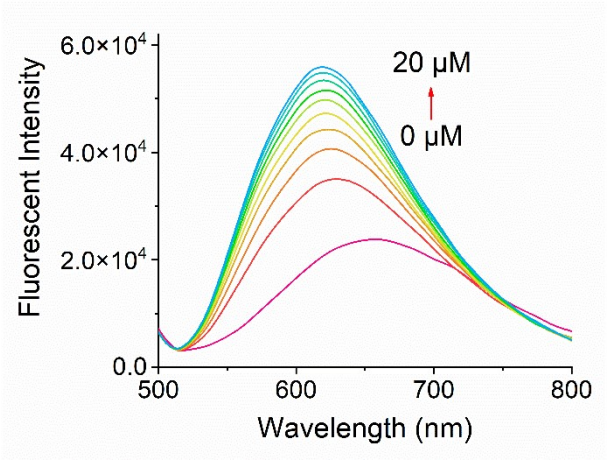

Fig. S17 Fluorescence spectra of **Rh-Mito** (10 μM) titrated with CT-DNA (0−20 μM) in Tris-HCl buffer (5 mM Tris-HCl, 50 mM NaCl, pH 7.4).

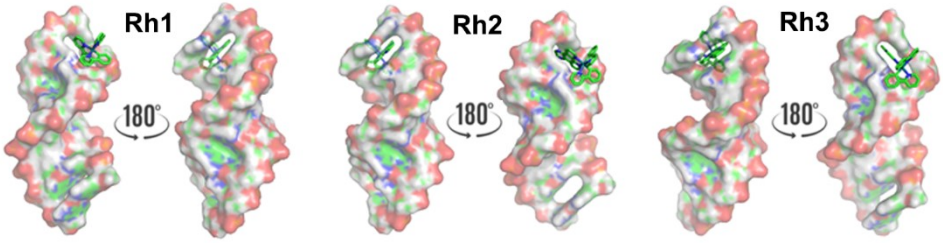

Fig. S18 Molecular docking studies of **Rh1**−**Rh3** with double-stranded DNA (PDB: 5IP8). The DNA fragment is shown in colors as a cartoon representation.

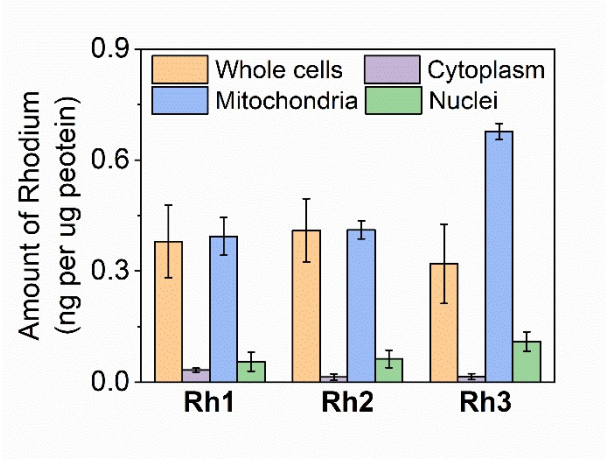

Fig. S19 Distribution of **Rh1**−**Rh3** (1.0 μM, 1 h) in cellular compartments of HeLa cells measured by ICP-MS.

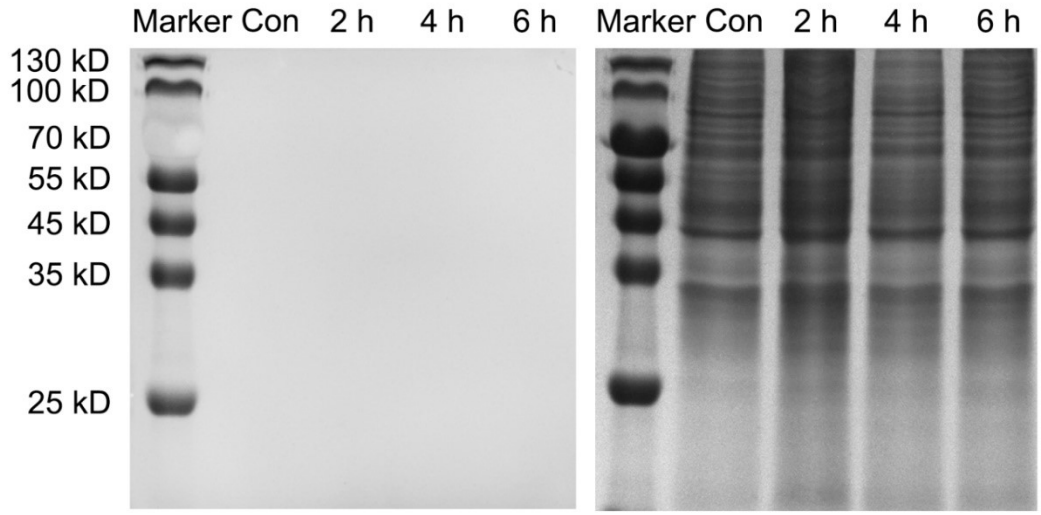

Fig. S20 SDS-PAGE analysis of proteins purified from **Rh-Mito**-treated HeLa cells. The cells were treated with **Rh-Mito** (1.0 μM) for 2 h, 4 h or 6 h at 37 °C. The gel was scanned with transmissive ultraviolet (λ_{ex} = 365 nm, Left) and then stained with CBB (Right).

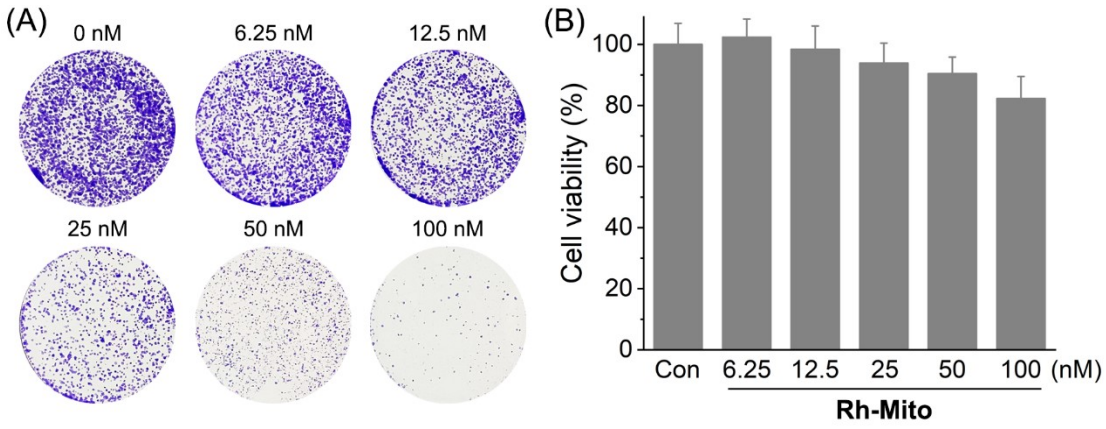

Fig. S21 (A) Inhibition of colony formation of HeLa cells by **Rh-Mito**. The cells were treated with **Rh-Mito** at the indicated concentrations for 7 days. (B) Cytotoxicity of **Rh-Mito** at the indicated concentrations for 7 days.

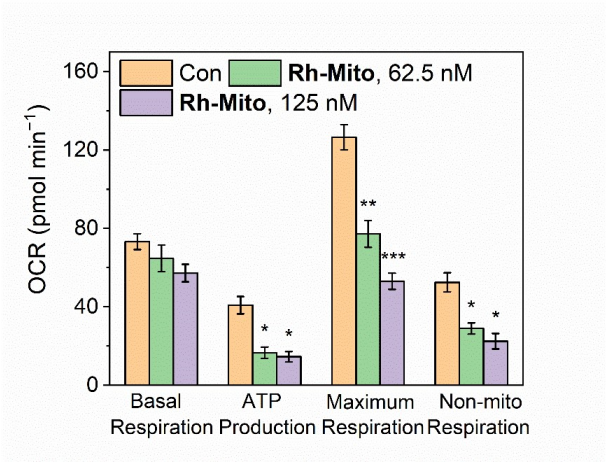

Fig. S22 The impact of **Rh-Mito** treatment (2 h) on OXPHOS: Basal cell respiration corresponds to the difference between OCR before the injection of oligomycin and OCR after the addition of a mixture of rotenone and antimycin A; ATP production values were obtained by subtracting OCR values after the addition of oligomycin from OCR values before the injection of oligomycin; Maximal cell respiration corresponds to the difference between OCR after the injection of FCCP and OCR after the addition of a mixture of rotenone and antimycin A; Non-mitochondrial cell respiration corresponds to the OCR values after the addition of a mixture of rotenone and antimycin A. *$p < 0.05$, **$p < 0.01$ and ***$p < 0.001$ by the Student's two-tailed t test.

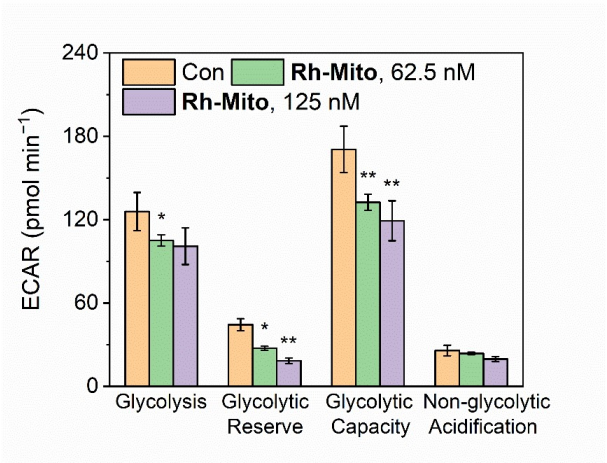

Fig. S23 The impact of **Rh-Mito** treatment (2 h) on glycolysis: Non-glycolytic acidification corresponds to the ECAR values before the injection of glucose; Glycolysis values were obtained by subtracting ECAR values before the addition of glucose from ECAR values after the injection of glucose; Glycolytic reserve

corresponds to the difference between ECAR after the injection of glucose and ECAR after the addition of oligomycin; Glycolyticcapacity were obtained by subtracting ECAR values before the addition of glucose from ECAR values after the injection of 2-DG. *$p < 0.05$, **$p < 0.01$ and ***$p < 0.001$ by the Student's two-tailed t test.

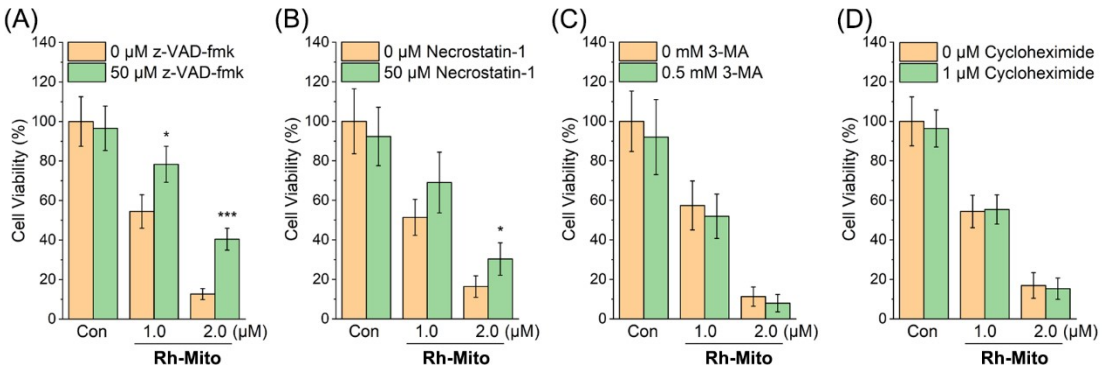

Fig. S24 Impact of different inhibitors on the antiproliferative activities of **Rh-Mito**. HeLa cells were treated with **Rh-Mito** at the indicated concentrations for 24 h in the absence or presence of inhibitors. *$p < 0.05$, **$p < 0.01$ and ***$p < 0.001$ by the Student's two-tailed t test.

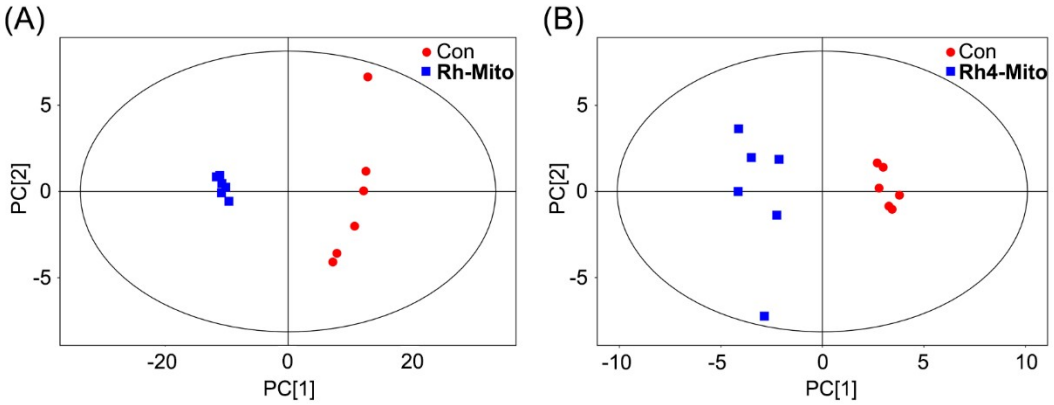

Fig. S25 PCA analysis of UHPLC-QTOFMS data in the (A) positive mode and (B) negative mode. PCA analysis shows that there is clear separation of the control group and the **Rh-Mito**-treated group (1.0 μM, 6 h).

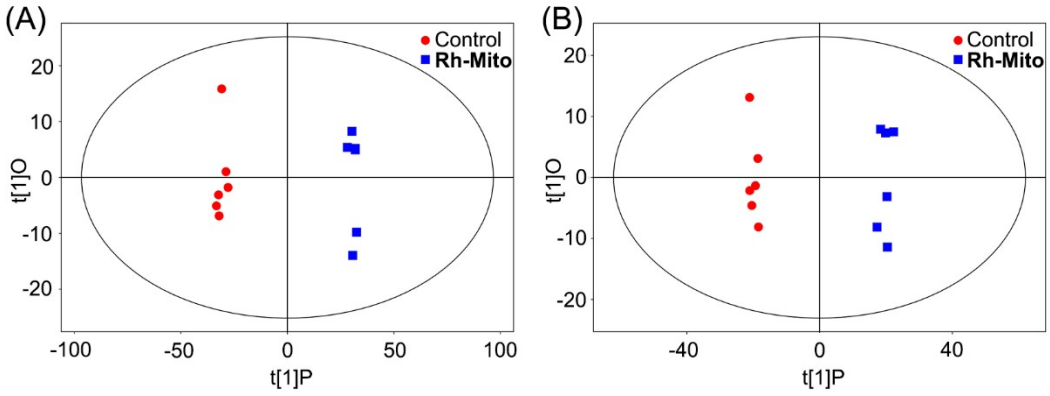

Fig. S26 OPLS-DA plots with the score of the first two principal components between control group and **Rh-Mito**-treated group (1.0 μM, 6 h) in the (A) positive mode and (B) negative mode.

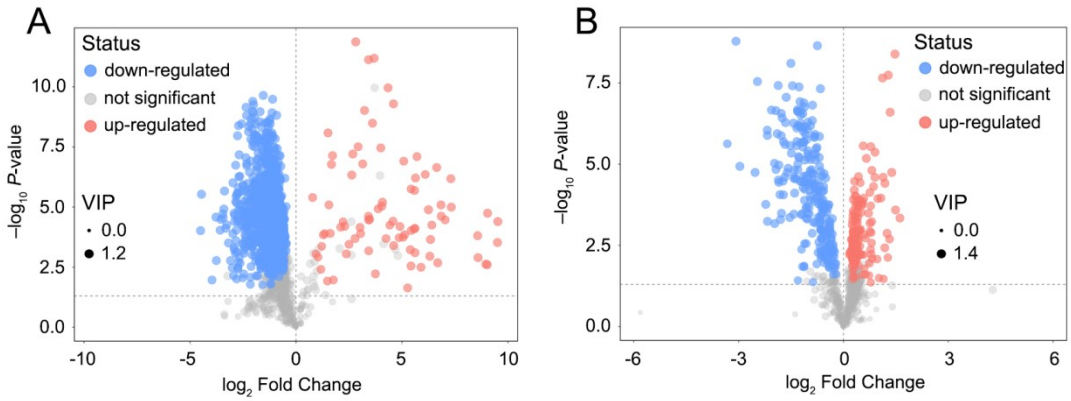

Fig. S27 Volcano plot for **Rh-Mito**-treated group (1.0 μM, 6 h) *vs* control group in the (A) positive mode and (B) negative mode. Standard: p-value < 0.05, VIP > 1.

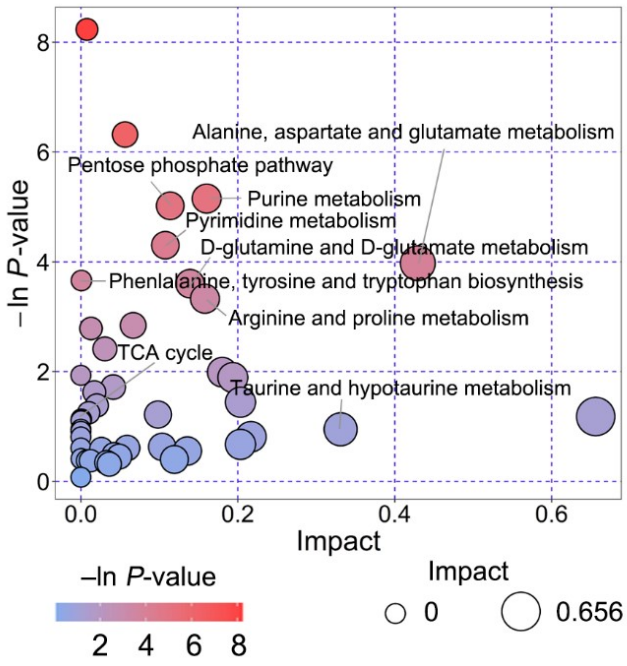

Fig. S28 Summary of metabolic pathway analysis of HeLa cells treated with **Rh-Mito** (1.0 μM, 6 h) in the negative mode. The colour of the circles means the *p*-value, and the area of the circles means pathway impact.

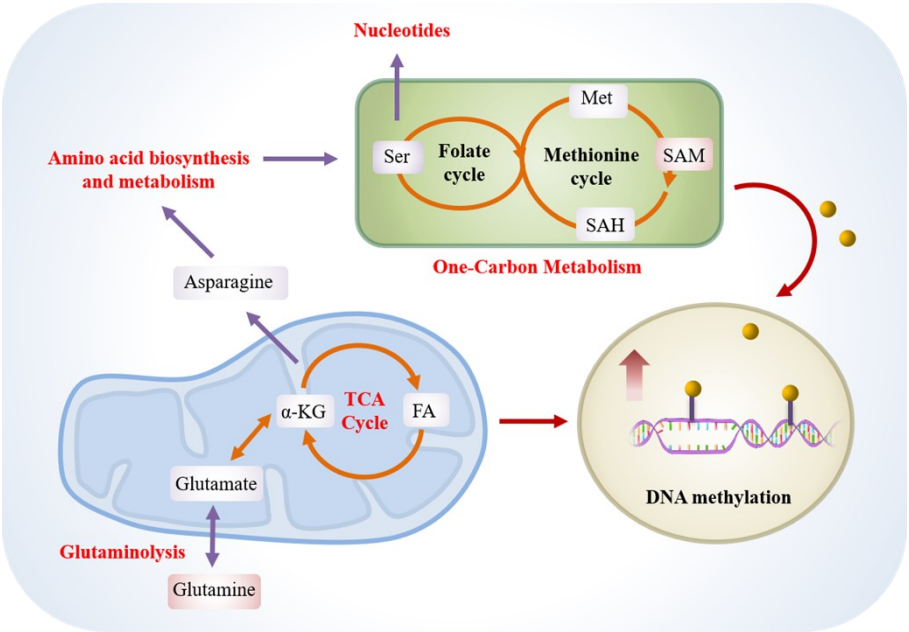

Fig. S29 The correlational regulation nets of differential metabolites upon **Rh-Mito** treatment (1.0 μM, 6 h).

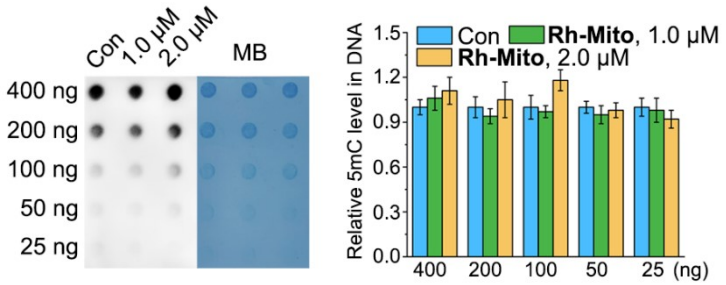

Fig. S30 Determination of the content of 5mC in DNA in HeLa-ρ0 cells treated with **Rh-Mito** for 6 h *via* dot blotting assay. *$p < 0.05$, **$p < 0.01$ and ***$p < 0.001$ by the Student's two-tailed t test.

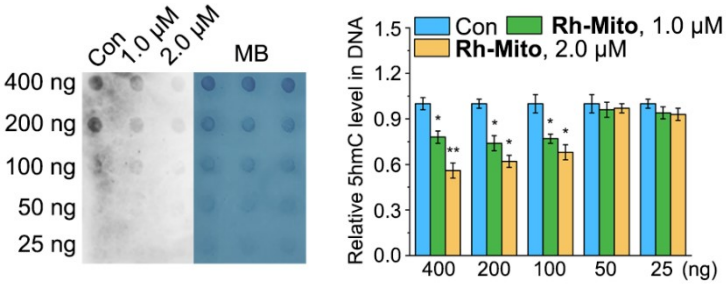

Fig. S31 Determination of the content of 5hmC in DNA in HeLa cells treated with **Rh-Mito** for 6 h *via* dot blotting assay. *$p < 0.05$, **$p < 0.01$ and ***$p < 0.001$ by the Student's two-tailed t test.

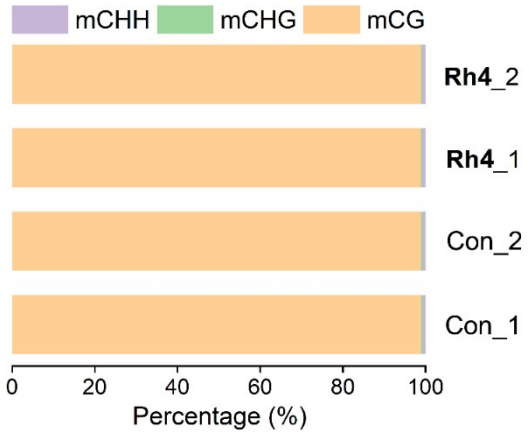

Fig. S32 Percentages of methylated C sites to total methylated C sites in different sequence contexts between the control and **Rh-Mito**-treated HeLa cells (1.0 μM, 6 h).

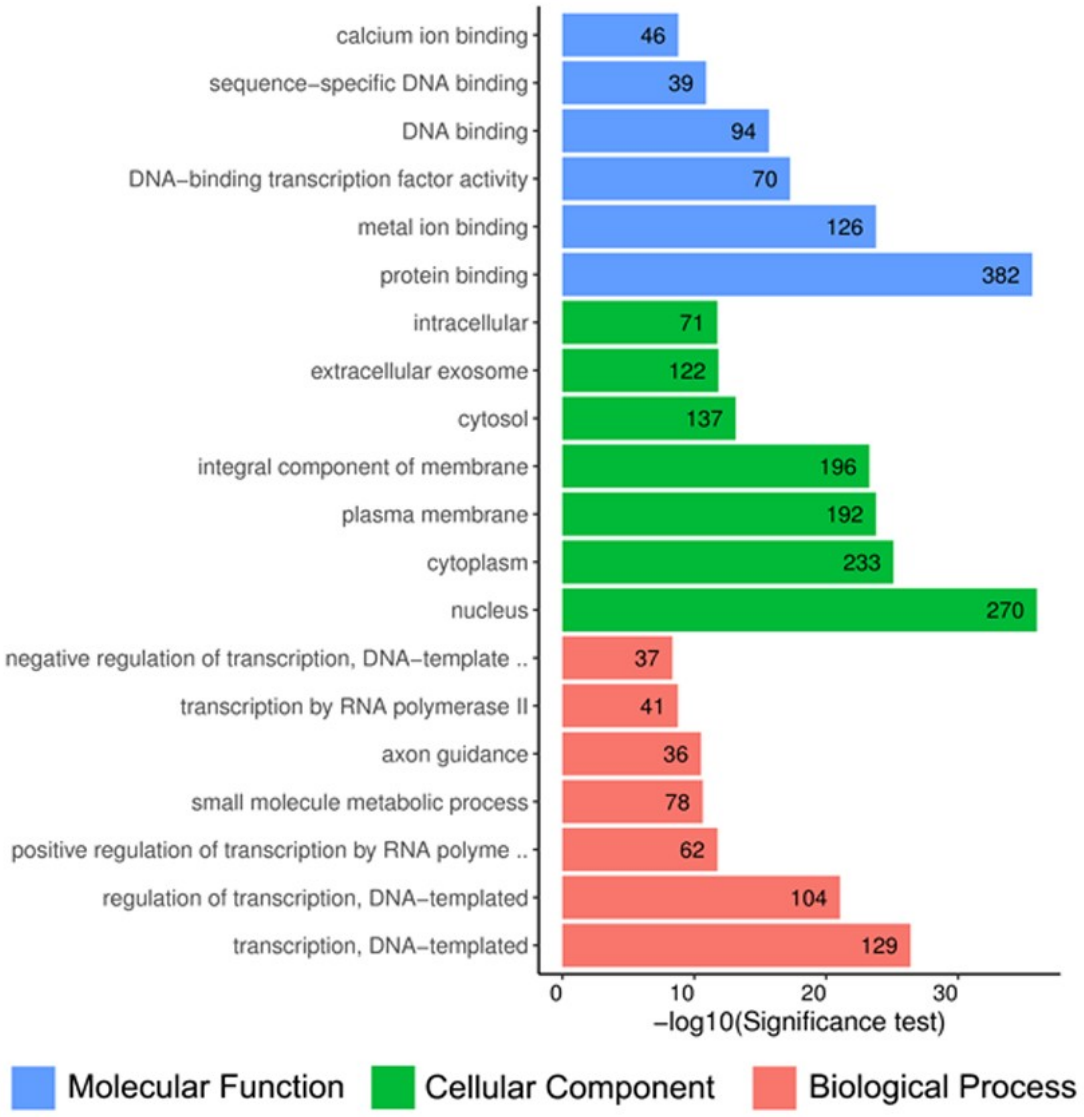

Fig. S33 GO categorization of molecular function, cellular component and biological process for DMRs in anchoring promoter regions induced by **Rh-Mito** treatment (1.0 μM, 6 h). Standard: Observed genes > 2, Fold change > 2 and False positive rate (FDR) < 0.05.

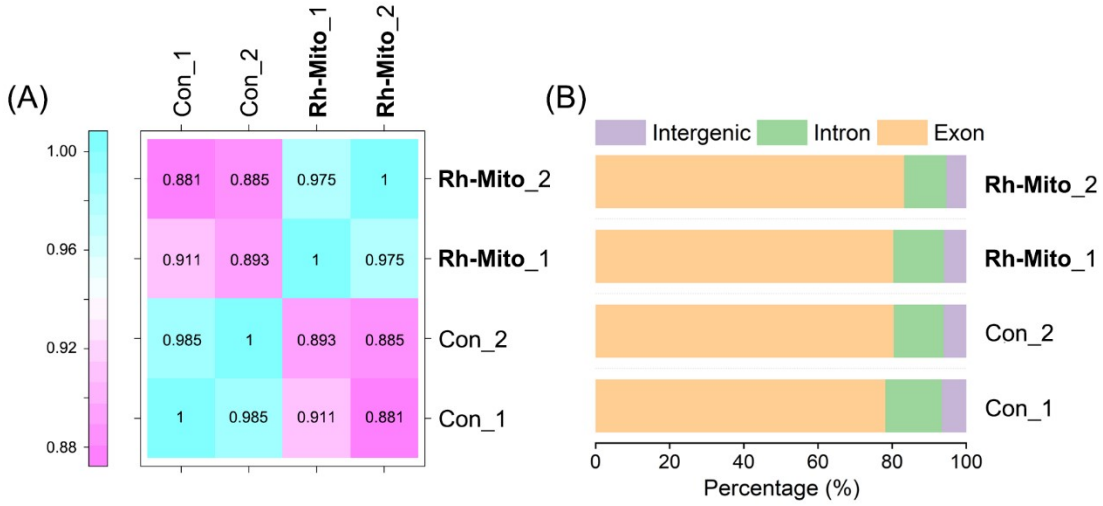

Fig. S34 (A) Heat map diagram of Pearson correlation coefficient between all samples. (B) The genomic location of mapped transcripts in control- *vs* **Rh-Mito**-treated HeLa cells (1.0 μM, 6 h).

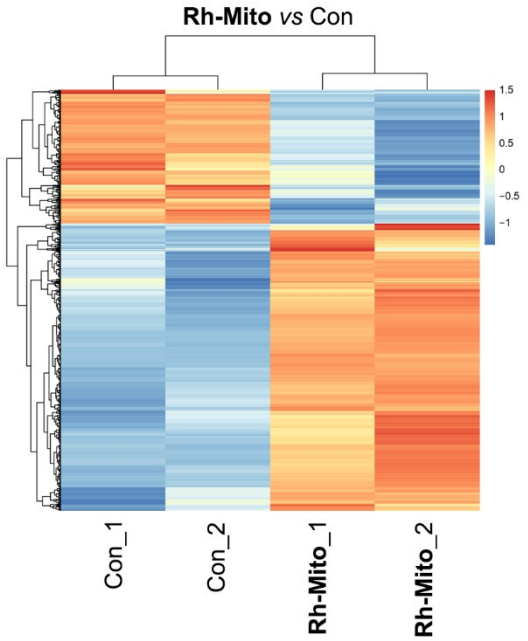

Fig. S35 Cluster analysis and Heatmap displays the overview of the differentially expressed genes induced by **Rh-Mito** treatment (1.0 μM, 6 h). Each column represents a sample, and each row represents a gene. Colours represent the expression level of the genes.

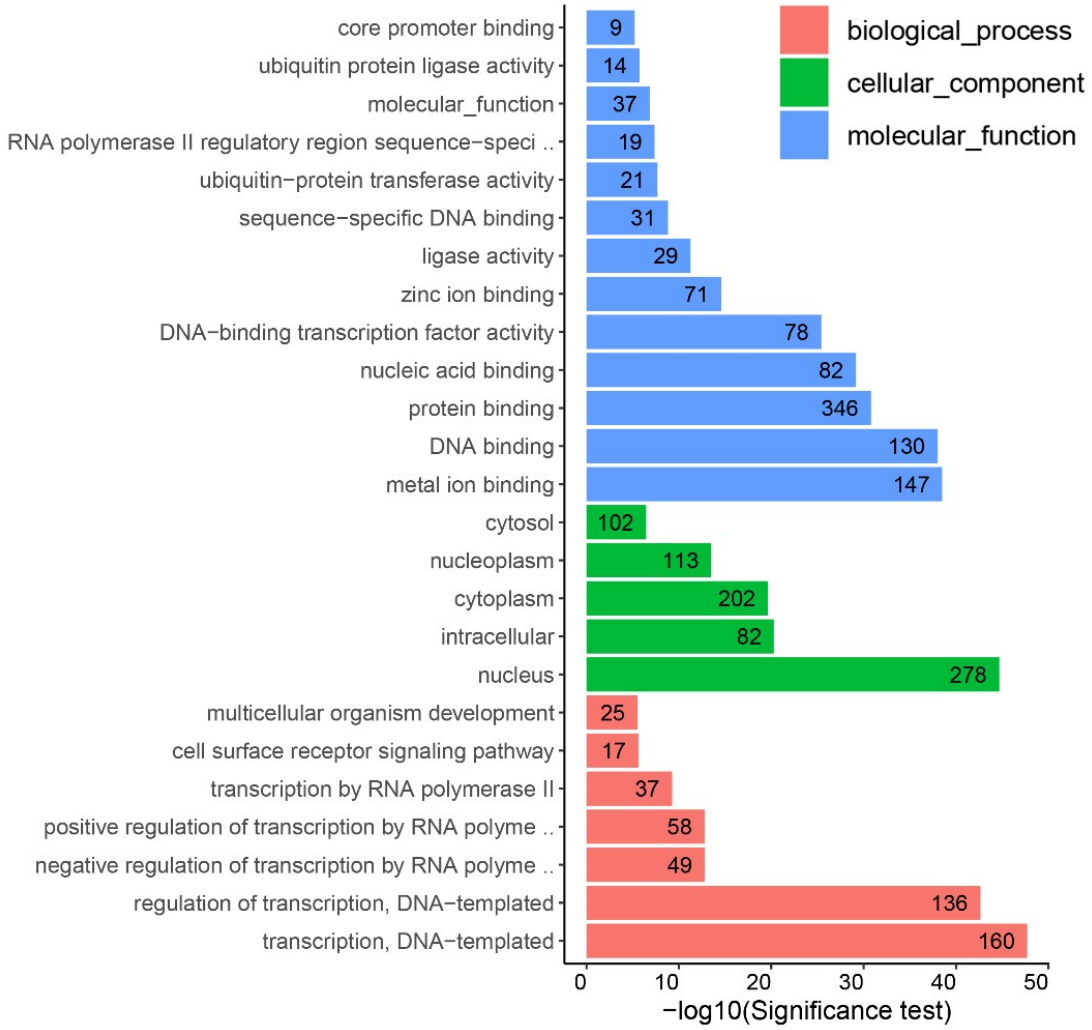

Fig. S36 GO categorization of molecular function, cellular component and biological process for assembled unigenes of the transcriptome upon **Rh-Mito** treatment (1.0 μM, 6 h). Standard: Observed genes > 2, Fold change > 2 and FDR < 0.05.

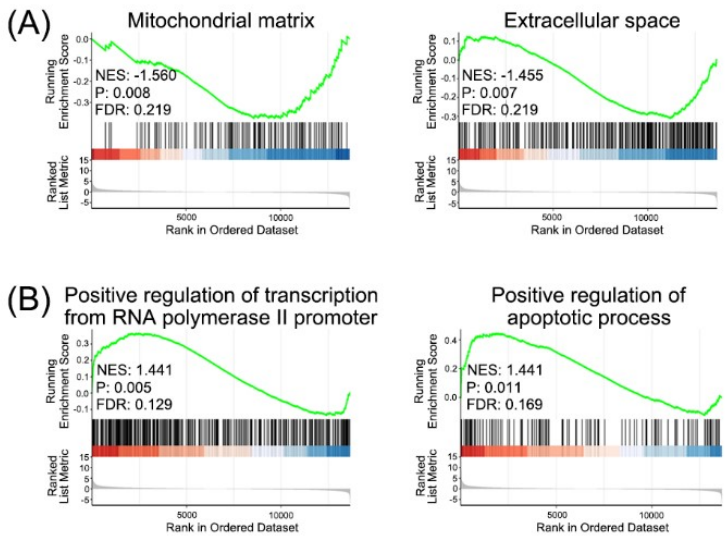

Fig. S37 GSEA reveals negative (A) and positive (B) enrichment of **Rh-Mito**-altered genes in various cellular processes. NES: normalized enrichment score. FDR: false positive rate.

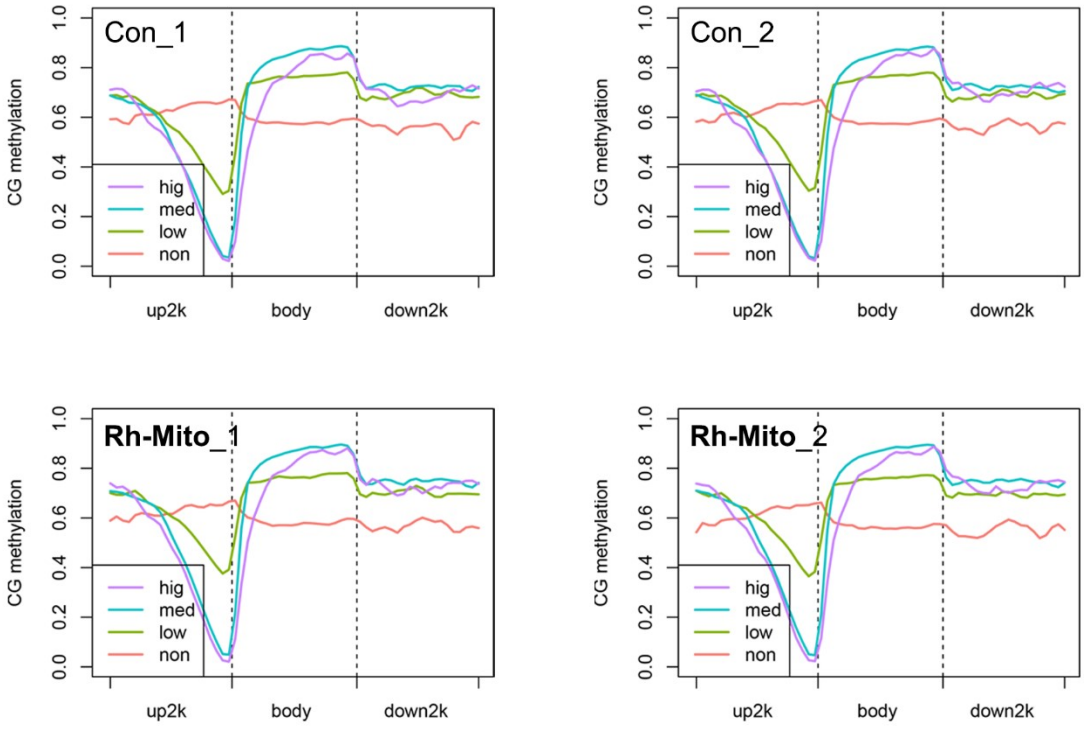

Fig. S38 Correlation between DNA methylated level and gene expressed level in the control group and **Rh-Mito**-treated group (1.0 μM, 6 h).

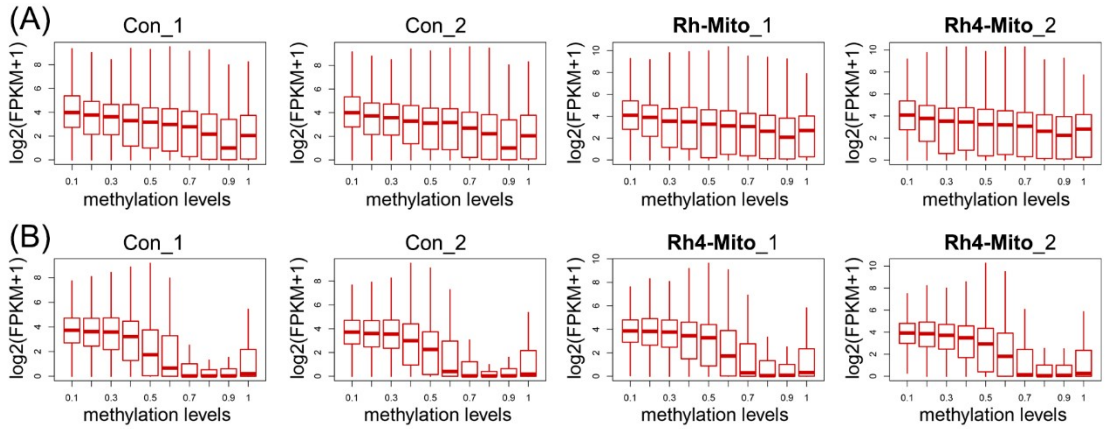

Fig. S39 Correlation between DNA methylated level and gene expressed level of (A) gene body and (B) promoter regions in the control group and **Rh-Mito**-treated group (1.0 μM, 6 h).

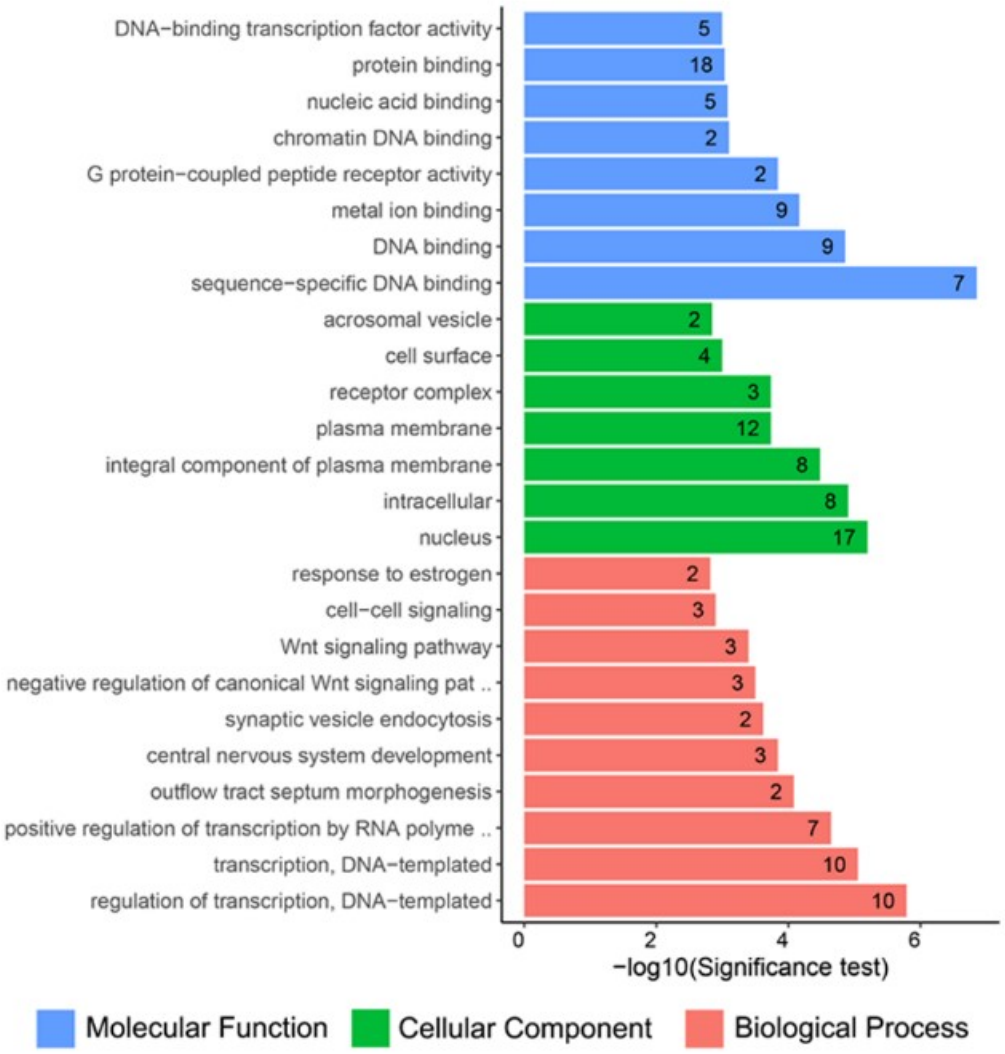

Fig. S40 GO categorization of molecular function, cellular component and biological process for DEGs with DMRs in anchoring promoter regions induced by **Rh-Mito** treatment (1.0 μM, 6 h). Standard: Observed genes > 2, Fold change > 2 and FDR < 0.05.

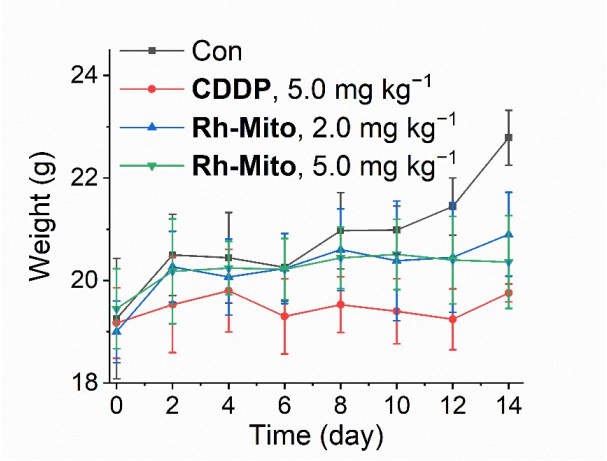

Fig. S41 Body weight of mice.

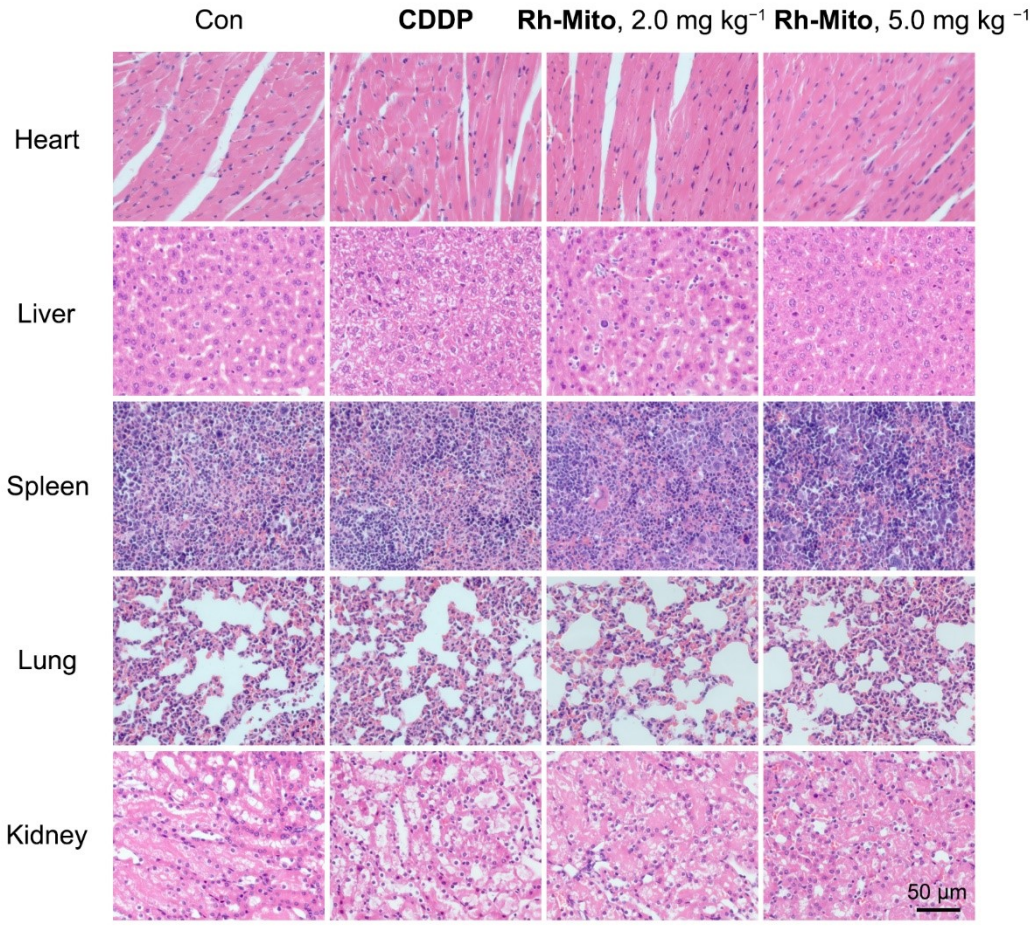

Fig. S42 H&E staining of organs at the end of treatment.

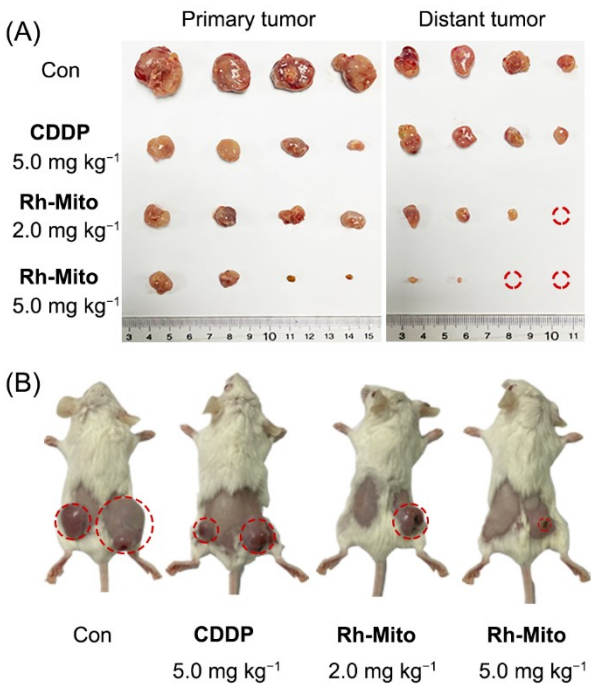

Fig. S43 (A) Represented images of tumorous sections (B) Represented images of tumor-bearing mice at the end of treatment.

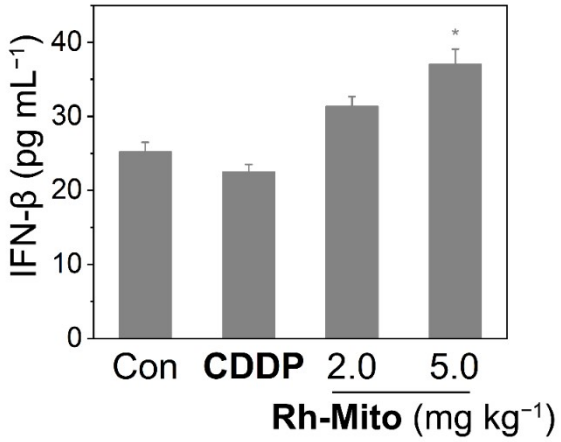

Fig. S44 ELISA showing increased type I IFNs (IFNβ) in serum after different treatments. *$p < 0.05$, **$p < 0.01$ and ***$p < 0.001$ by the Student's two-tailed t test.

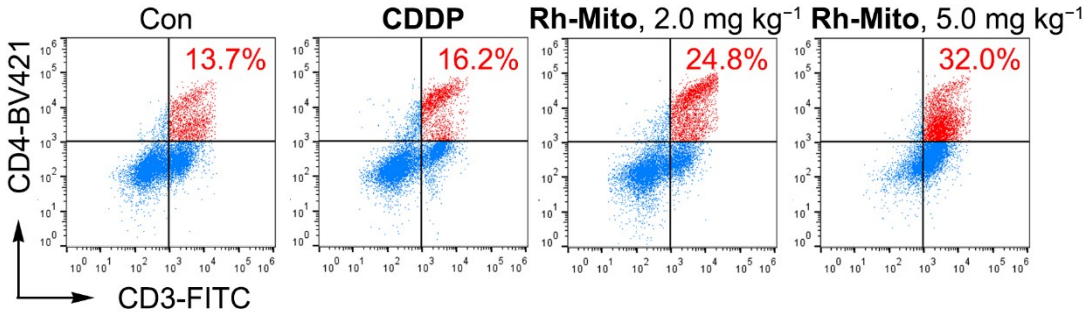

Fig. S45 Populations of $CD4^+$T cells in tumors after different treatments (n=3).

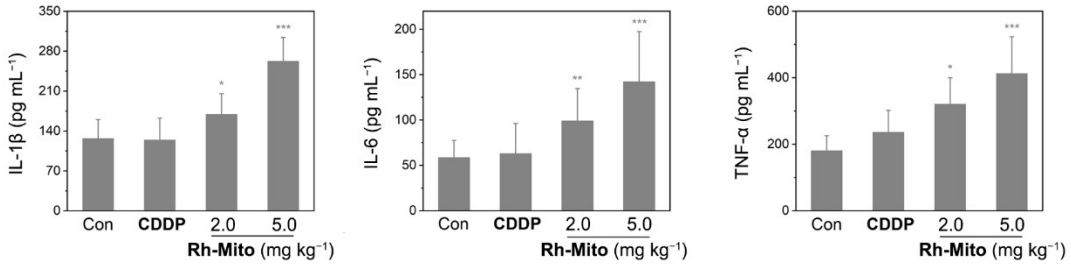

Fig. S46 Secretion of cytokines in serum measured by ELISA assay (n = 3) after different treatments. *$p < 0.05$, **$p < 0.01$ and ***$p < 0.001$ by the Student's two-tailed t test.

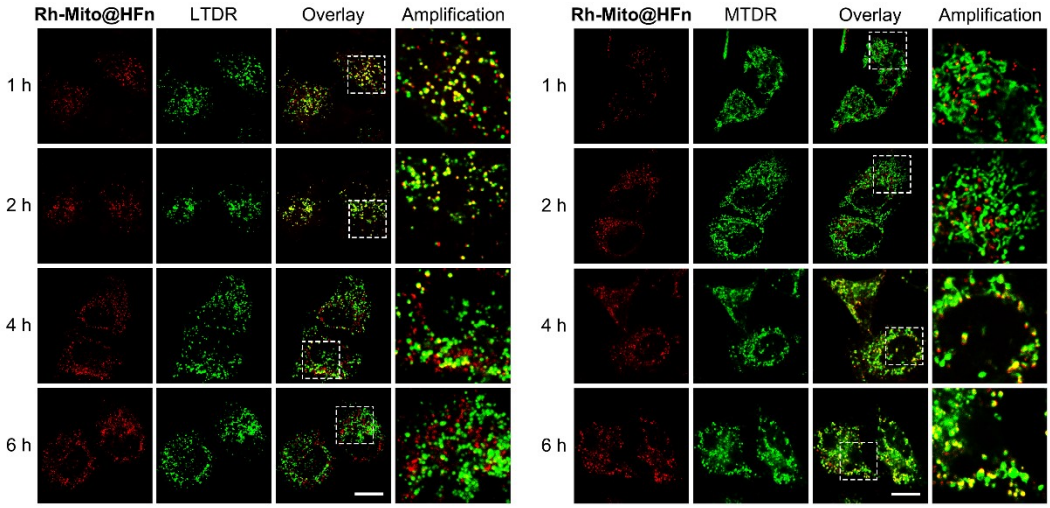

Fig. S47 Confocal microscopic images of Hela cells incubated with **Rh-Mito@HFn** (1.0 μM) at different time intervals (**Rh-Mito@HFn**, λ_{ex} = 405 nm, λ_{em} = 650 ± 20 nm; LTDR, λ_{ex} = 633 nm, λ_{em} = 660 ± 20 nm). Scale bar: 10 μm.

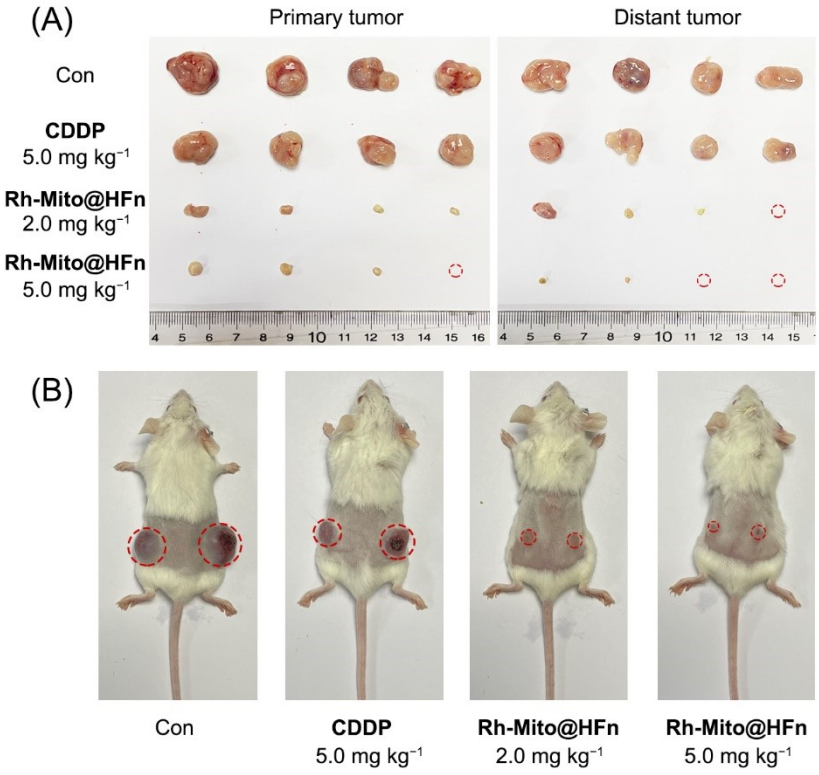

Fig. S48 (A) Represented images of tumor sections. (B) Represented images of tumor-bearing mice at the end of treatment.

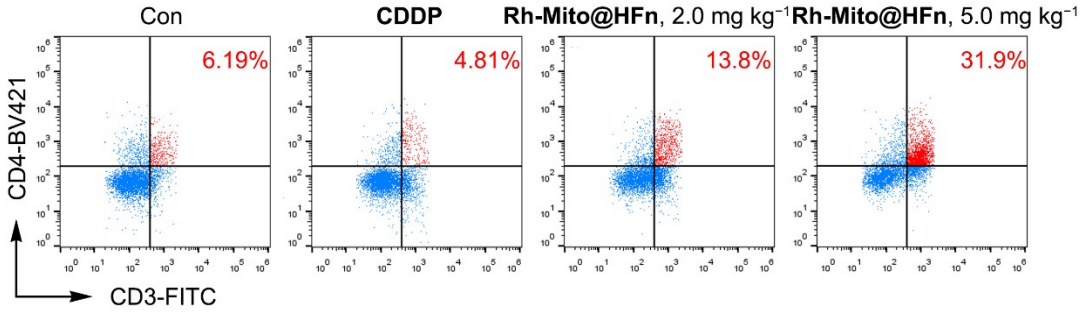

Fig. S49 Populations of $CD4^+$T cells in tumors after different treatments (n=3).

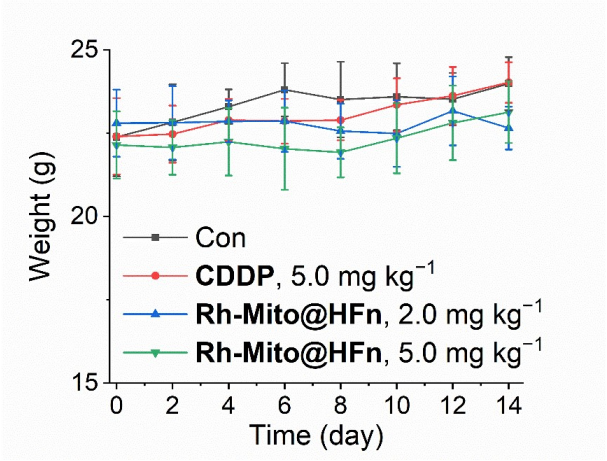

Fig. S50 Body weight of mice.

Supplementary Tables

Table S1 Photophysical data of **Rh-Mito** in different degassed solvents[a]

Solvent	$\lambda_{ex,\ max}$ (nm)	$\lambda_{em,\ max}$ (nm)	Φ_{em}[b]	Lifetime (ns)
PBS	420	604	0.07%	4.61
CH_2Cl_2	420	596	0.69%	6.46
CH_3CN	416	604	1.07%	8.37

[a] Concentrations of **Rh-Mito** were 10 μM.

[b] Degassed solvent of $[Ru(bpy)_3]^{2+}$ were used as standard, PBS (Φ_{em} = 0.042)[13], CH_2Cl_2 (Φ_{em} = 0.059)[14] and CH_3CN (Φ_{em} = 0.062)[15].

Table S2 Lipophilicity and cellular uptake efficiency of rhodium(III) complexes

Complex	Lipophilicity (log $P_{o/w}$)	Amount of rhodium (ng/10^5 cells)				
		HeLa	A549	MCF-7	HepG2	MCF-10A
Rh1	1.44	18.9±1.4	20.6±3.1	13.8±2.9	16.6±1.6	16.4±1.6
Rh2	1.99	22.5±3.8	28.8±3.9	19.2±2.1	19.4±1.5	20.3±1.3
Rh3	2.01	36.5±2.6	36.2±2.4	29.6±5.2	24.4±1.8	20.5±1.6
Rh-Mito	2.54	44.3±5.5	38.1±4.3	36.7±4.3	28.6±2.0	7.2±0.9

Table S3 Cellular uptake mechanism of **Rh-Mito**

Complex	Amount of rhodium (ng/10^5 cells)			
	37 °C	4 °C	CCCP	Chloroquine
Rh-Mito	40.9±4.8	16.5±2.7	21.4±2.9	37.6±4.1

Table S4 Antiproliferative activity (IC_{50} values) of referenced complexes **Rh1**−**Rh3** against different cell lines[a]

Complexes	IC_{50} (μM)								
	HeLa	HeLa-ρ0 (MTFs)	MCF-7	MB-MDA-231	A549	NCI-H1299	HepG2	MCF-10A	HLF
Rh1	1.6±0.2	1.2±0.5 (0.8)	6.1±0.8	7.9±0.8	2.9±0.4	4.6±0.4	10.6±1.2	4.8±0.6	5.5±0.6
Rh2	0.9±0.1	2.1±0.4 (2.3)	1.9±0.2	3.4±0.5	1.1±0.2	0.7±0.2	3.7±0.7	3.1±0.3	5.8±0.9
Rh3	0.4±0.1	2.3±0.3 (5.7)	0.5±0.1	1.1±0.1	0.7±0.1	0.4±0.1	2.0±0.3	2.6±0.2	3.6±0.5

[a] Data are presented as the means ± standard deviations (SD), and antiproliferative activity was assessed after 72 h of incubation.

Table S5 Cell viabilities (CC_{50}) of **Rh-Mito** against different cell lines[a]

Complex	CC_{50} (μM)				
	HeLa	MB-MDA-231	A549	HepG2	MCF-10A
Rh-Mito	0.5±0.1	1.0±0.2	0.8±0.1	1.5±0.3	3.3±0.4

[a] Data are presented as the means ± standard deviations (SD), and cell viabilities were assessed after 72 h of incubation.

Table S6 Primer sequences of the selected genes studied in PCR

Appellative	Sequence
CYTb-F	ACCCCCTAGGAATCACCTCC
CYTb-R	GCCTAGGAGGTCTGGTGAGA
ND6-F	GGAGGATCCTATTGGTGCGG
ND6-R	CCTATTCCCCCGAGCAATCTC
ND5-F	TGGCAGCCTAGCATTAGCAG
ND5-R	GATAGGGCTCAGGCGTTTGT
ND4-F	ACACAATGGGGCTCACTCAC
ND4-R	CCGGTAATGATGTCGGGGTT
ND4L-F	TACTAGTTTTTGCCGCCTGC
ND4L-R	AGCATTGGAGTAGGCTTAGGTT
ND3-F	GCCCTCCTTTTACCCTTACCA
ND3-R	GGCCAGACTTAGGGCTAGGA
COX3-F	ACCCTCCTACAAGCCTCAGA
COX3-R	TGACGTGAAGTCCGTGGAAG
ATPase6-F	GAAGCGCCACCCTAGCAATA
ATPase6-R	GCTTGGATTAAGGCGACAGC
ATPase8-F	CACAAACTACCACCTACCTCCC
ATPase8-R	GGGCAATGAATGAAGCGAAC
COX2-F	GCTGTCCCCACATTAGGCTT

COX2-R	ACCGTAGTATACCCCCGGTC
COX1-F	CCCCGATGCATACACCACAT
COX1-R	TCGAAGCGAAGGCTTCTCAA
ND2-F	AGCACCACGACCCTACTACT
ND2-R	CATTTGGGCAAAAAGCCGGT
ND1-F	TAACGCACTCTCCCCTGAAC
ND1-R	GTAGCGGAATCGGGGGTATG
mtDNA-F	CAC CCA AGA ACA GGG TTT GT
mtDNA-R	TGG CCA TGG GTA TGT TGT TA
nDNA-F	TGC TGT CTC CAT GTT TGA TGT ATC T
nDNA-R	TCT CTG CTC CCC ACC TCT AAG T
8.9-kb segment-F	TCTAAGCCTCCTTATTCGAGCCGA
8.9-kb segment-R	TTTCATCATGCGGAGATGTTGGATGG
12.2-kb segment-F	CATGTCACCACTGGACTCTGAAC
12.2-kb segment-R	CCTGGAGTAGGAACAAAATTGCT
FOXQ1-F	CCCATAGTCCACCCAACAC
FOXQ1-R	TGGTCTTCCGAGATAGTCACT
THSD1-F	CAACAGACAACAGCACTC
THSD1-R	CCTTGGCACTCCTATTCA
SOX17-F	GCGGTATATTACTGCAACTATC
SOX17-R	TCCTCCAGGAAGTGTGTA

CD24-F	CCCAAATCCAACTAATGCC
CD24-R	GAGACCACGAAGAGACTG
NPTX1-F	GAGGTTCAGTCATTCCAGTG
NPTX1-R	CAAGACACAGGTTCACCATAA
TOLLIP-F	CCTGGTCTTACGCCTGTGTAG
TOLLIP-R	GGTCTGTCCTGGGTTAGAGTTG
PRICKLE1-F	GCAGAACCCAGGAATGAATCG
PRICKLE1-R	GAGGAGGAGGAGGAAGAACAC
FOXO3-F	CCAGCACCAAGTCTACGG
FOXO3-R	GACCAACACTGTTCACATTAGC
TMEM88-F	GGAGCAGCAGCGTCAGTG
TMEM88-R	GGTCGTGAAAGGAAAGTGGGTTT
FJX1-F	TTGCGTTTGAGCCGTTGAG
FJX1-R	TCCACCAGCCAATGTCACA
actin-F	CTCCATCCTGGCCTCGCTGT
actin-R	GCTGTCACCTTCACCGTTCC

Table S7 GO terms enrichment analysis for immune- and cancer-related genes for **Rh-Mito**-treatment groups [a]

Genes	Official Full Name	Functions
THSD1	thrombospondin type 1 domain containing 1	The protein encoded by this gene contains a type 1 thrombospondin domain, which is found in a number of proteins involved in the complement pathway, as well as in extracellular matrix proteins. Alternatively spliced transcript variants encoding different isoforms have been observed for this gene. This gene is also validated as tumor-suppressive gene.
FOXQ1	forkhead box Q1	FOXQ1 is a member of the FOX gene family, which is characterized by a conserved 110-amino acid DNA-binding motif called the forkhead or winged helix domain. FOX genes are involved in embryonic development, cell cycle regulation, tissue-specific gene expression, cell signaling, and tumorigenesis.
SOX17	SRY-box transcription factor 17	This gene encodes a member of the SOX (SRY-related HMG-box) family of transcription factors involved in the regulation of embryonic development and in the determination of the cell fate. The encoded protein may act as a transcriptional regulator after forming a protein complex with other proteins. This gene is also validated as tumor-suppressive and DNA repair-inhibitive gene.

FOXO3	forkhead box O3	This gene belongs to the forkhead family of transcription factors which are characterized by a distinct forkhead domain. This gene likely functions as a trigger for apoptosis through expression of genes necessary for cell death. Translocation of this gene with the MLL gene is associated with secondary acute leukemia. Alternatively spliced transcript variants encoding the same protein have been observed.
NPTX1	neuronal pentraxin 1	NPTX1 is a member of the neuronal pentraxin gene family. Neuronal pentraxin 1 is similar to the rat NP1 gene which encodes a binding protein for the snake venom toxin taipoxin. Human NPTX1 mRNA is exclusively localized to the nervous system. This gene is also associated with carcinogenesis and metastasis.
PRICKLE1	prickle planar cell polarity protein 1	This gene encodes a nuclear receptor that may be a negative regulator of the Wnt/beta-catenin signaling pathway. The encoded protein localizes to the nuclear membrane and has been implicated in the nuclear trafficking of the transcription repressors REST/NRSF and REST4. Mutations in this gene have been linked to progressive myoclonus epilepsy. Alternate splicing results in multiple transcript variants. A pseudogene of this gene is found

		on chromosome 3.
TMEM88	transmembrane protein 88	Predicted to enable PDZ domain binding activity. Involved in negative regulation of canonical Wnt signaling pathway; protein localization to plasma membrane; and protein stabilization. Located in cytosol and plasma membrane.
TOLLIP	toll interacting protein	This gene encodes a ubiquitin-binding protein that interacts with several Toll-like receptor (TLR) signaling cascade components. The encoded protein regulates inflammatory signaling and is involved in interleukin-1 receptor trafficking and in the turnover of IL1R-associated kinase. Several transcript variants encoding different isoforms have been found for this gene.
CD24	CD24 molecule	This gene encodes a sialoglycoprotein that is expressed on mature granulocytes and B cells and modulates growth and differentiation signals to these cells. The precursor protein is cleaved to a short 32 amino acid mature peptide which is anchored via a glycosyl phosphatidylinositol (GPI) link to the cell surface. This gene was missing from previous genome assemblies, but is properly located on chromosome 6. Non-transcribed pseudogenes have been designated on chromosomes 1, 15, 20, and Y. Alternative splicing results in

		multiple transcript variants. CD24 signalling through macrophage Siglec-10 is a target for cancer immunotherapy.
FJX1	four-jointed box kinase 1	The protein encoded by this gene is the human ortholog of mouse and Drosophila four-jointed gene product. The Drosophila protein is important for growth and differentiation of legs and wings, and for proper development of the eyes. This gene is also validated as oncogene.

[a] Information of above genes are acquired from National Center for Biotechnology Information (NCBI).

List of the other Supplementary Data

Supplementary Data S1*: The most prominent metabolites in the positive mode.*

Supplementary Data S2*: The most prominent metabolites in the negative mode.*

Supplementary Data S3*: Differentially methylated regions in promotors in HeLa cells treated with* ***Rh-Mito****.*

Supplementary Data S4*: Differentially expressed genes identified by RNA-seq in HeLa cells treated with* ***Rh-Mito****.*

Supplementary Data S5: *The integration analysis of RRBS and RNA-seq.*

Supplementary Data S6: *Raw images of blots and gels.*

References

1. S. Sprouse, K. A. King, P. J. Spellane and R. J. Watts, *J. Am. Chem. Soc.*, 1984, **106**, 6647-6653.
2. G. Che, W. Li, Z. Kong, Z. Su, B. Chu, B. Li, Z. Zhang, Z. Hu and H. Chi, *Synth. Commun.*, 2006, **36**, 2519-2524.
3. W. J. Wang, X. Mu, C. P. Tan, Y. J. Wang, Y. Zhang, G. Li and Z. W. Mao, *J. Am. Chem. Soc.*, 2021, **143**, 11370-11381.
4. J. J. Cao, Y. Zheng, X. W. Wu, C. P. Tan, M. H. Chen, N. Wu, L. N. Ji and Z. W. Mao, *J. Med. Chem.*, 2019, **62**, 3311-3322.
5. Y.-Y. Ling, X.-Y. Xia, L. Hao, W.-J. Wang, H. Zhang, L.-Y. Liu, W. Liu, Z.-Y. Li, C.-P. Tan and Z.-W. Mao, 2022, **61**, e202210988.
6. S. Su, J. Liao, J. Liu, D. Huang, C. He, F. Chen, L. Yang, W. Wu, J. Chen, L. Lin, Y. Zeng, N. Ouyang, X. Cui, H. Yao, F. Su, J. D. Huang, J. Lieberman, Q. Liu and E. Song, *Cell Res.*, 2017, **27**, 461-482.
7. J. J. Cao, C. P. Tan, M. H. Chen, N. Wu, D. Y. Yao, X. G. Liu, L. N. Ji and Z. W. Mao, *Chem. Sci.*, 2017, **8**, 631-640.
8. C. X. Song, K. E. Szulwach, Y. Fu, Q. Dai, C. Yi, X. Li, Y. Li, C. H. Chen, W. Zhang, X. Jian, J. Wang, L. Zhang, T. J. Looney, B. Zhang, L. A. Godley, L. M. Hicks, B. T. Lahn, P. Jin and C. He, *Nat. Biotechnol.*, 2011, **29**, 68-72.
9. A. Meissner, A. Gnirke, G. W. Bell, B. Ramsahoye, E. S. Lander and R. Jaenisch, *Nucleic Acids Res.*, 2005, **33**, 5868-5877.
10. H. Gu, Z. D. Smith, C. Bock, P. Boyle, A. Gnirke and A. Meissner, *Nat. Protoc.*, 2011, **6**, 468-481.
11. M. Liang, H. Tan, J. Zhou, T. Wang, D. Duan, K. Fan, J. He, D. Cheng, H. Shi, H. S. Choi and X. Yan, *ACS Nano*, 2018, **12**, 9300-9308.
12. J. Zhang, D. Cheng, J. He, J. Hong, C. Yuan and M. Liang, *Nat. Protoc.*, 2021, **16**, 4878-4896.

13. J. Van Houten and R. J. Watts, *J. Am. Chem. Soc.*, 1976, **98**, 4853-4858.

14. D. Pucci, A. Bellusci, A. Crispini, M. Ghedini, N. Godbert, E. I. Szerb and A. M. Talarico, *J. Mater. Chem.*, 2009, **19**.

15. Daniel S. Tyson and F. N. Castellano, *J. Phys. Chem. A*, 1999, **103**, 10955-10960.